CD1a on Langerhans cells controls inflammatory skin diseases

Ji Hyung Kim[1†], Yu Hu[1†], Tang Yongqing[2,3], Jessica Kim[1], Victoria A. Hughes[2,3], Jérôme Le Nours[2,3], Elsa A. Marquez[2,3], Anthony W. Purcell[2], Qi Wan[1], Masahiko Sugita[4], Jamie Rossjohn[2,3,5†]* & Florian Winau[1†]*

[1] Program in Cellular and Molecular Medicine, Boston Children's Hospital, Department of Microbiology and Immunobiology, Harvard Medical School, Boston, USA

[2] Infection and Immunity Program & Department of Biochemistry and Molecular Biology, Biomedicine Discovery Institute, Monash University, Clayton, Victoria 3800, Australia

[3] Australian Research Council Centre of Excellence in Advanced Molecular Imaging, Monash University, Clayton, Victoria 3800, Australia

[4] Laboratory of Cell Regulation, Institute for Virus Research, Kyoto University, Kyoto, Japan

[5] Institute of Infection and Immunity, Cardiff University, School of Medicine, Heath Park, Cardiff, CF14 4XN, UK

*Correspondence to: jamie.rossjohn@monash.edu, or florian.winau@childrens.harvard.edu

†These authors contributed equally to this work.

ABSTRACT

CD1a is a lipid-presenting molecule abundantly expressed on Langerhans cells. However, the in vivo role of CD1a remains unclear, principally because CD1a is lacking in mice. Using CD1a-transgenic mice, we show that urushiol from poison ivy triggers CD1a-dependent skin inflammation, driven by CD4 T cells producing IL-17 and IL-22. Notably, human subjects with poison ivy dermatitis showed a similar cytokine signature following CD1a-mediated urushiol recognition. Among different urushiol congeners, we identified diunsaturated pentadecylcatechol (C15:2) as the dominant antigen for CD1a-restricted T cells. We determined the crystal structure of the CD1a-urushiol (C15:2) complex, demonstrating the molecular basis of urushiol interaction with the antigen-binding cleft of CD1a. In a mouse model and psoriasis patients, CD1a amplified inflammatory responses mediated by Th17 cells reactive with self lipid antigens. Remarkably, treatment with blocking antibodies against CD1a alleviated skin inflammation. Thus, we propose CD1a as a potential target for future therapeutic strategies against inflammatory skin diseases.

The family of CD1 molecules consists of group 1 CD1 (CD1a, b, c, and e) and group 2 CD1 (CD1d) proteins[1]. In contrast to MHC proteins that present peptides, CD1 molecules present lipid antigens to T lymphocytes[1-2]. For example, the CD1d molecule presents α-anomeric glycosphingolipids to invariant NKT cells[3], whereas CD1a-c molecules are mainly described to present lipids and lipopeptides from mycobacteria to a diverse T cell repertoire[4]. Notably, CD1a can display a broad spectrum of exogenous lipid antigens derived from pollen[5] or bacteria[6-8]. In addition, CD1a also presents self lipid antigens from host origin[9-15], such as triacylglycerol, squalene, wax ester, and fatty acid, which are enriched in the skin epidermis[9].

The abundant expression of CD1a hallmarks Langerhans cells in the skin. Langerhans cells originate from yolk-sac-derived fetal liver progenitors[16,17], require IL-34 for development[18], and constitute the principal dendritic cell (DC) subset in the epidermis[19,20]. Additionally, the dermis harbors dermal as well as langerin-positive DCs. The three DC types in the skin fulfill different functions in antigen presentation: Langerin-positive dermal DCs are important for cross-priming of CD8 T cells, whereas Langerhans cells preferably induce Th17 cells[21,22].

The intricate immune system of the skin is critically involved in responses to extrinsic insults like allergens[23], as well as in autoimmune diseases, such as psoriasis[24,25]. Contact dermatitis is a common skin disease caused by exposure to small organic or inorganic molecules[23]. During the sensitization phase, allergen-specific T lymphocytes are generated that mediate skin inflammation upon challenge with the same antigen[23]. The sap compound urushiol of the plant poison ivy can trigger severe inflammation, and urushiol-specific T cells have been implicated in this process in the human system[26-28]. Psoriasis is a chronically relapsing, T cell-mediated inflammatory skin disease with a prevalence of 2-3% worldwide[24,25]. The disease is characterized by epidermal thickening (acanthosis), which leads to itchy and scaling plaques on

the macroscopic level[24,25]. Importantly, it is well known that the cytokines IL-17 and IL-22 are crucial for the development of psoriasis[25]. Although psoriasis is considered an autoimmune disease, the nature of the antigens recognized remain elusive[25].

Considering that Langerhans cells predominantly express CD1a and reside in the epidermis that is readily accessible to foreign as well as self lipid antigens, Langerhans cells and CD1a-restricted T cells are prime candidates for regulating skin immunity. However, since CD1a is expressed in humans but lacking in mice[1], the in vivo functions of CD1a on Langerhans have not been addressed and remain unclear.

Here, we show the vital importance of Langerhans cells expressing CD1a in skin inflammation in vivo. To demonstrate a role of CD1a on Langerhans cells in the induction of inflammatory skin diseases, we used human CD1a-transgenic mice and found that CD1a drives pathogenesis of poison ivy dermatitis and psoriasis. Furthermore, we showed that CD1a-mediated skin inflammation is abrogated by CD1a blocking antibodies, highlighting CD1a as a novel target for treatment of inflammatory skin diseases.

RESULTS

CD1a promotes Th17-mediated skin inflammation in response to poison ivy

Based on its lipophilic nature and the chemical structure of pentadecylcatechol, we hypothesized that urushiol could represent a ligand displayed by the lipid-presenting molecule CD1a to cause inflammation. To this end, we sensitized and challenged CD1a-transgenic (CD1aTg) or wild-type (WT) mice with urushiol applied to the skin (30 µl of 20 mg/ml for sensitization; 10 µl of 5 mg/ml for challenge). Ear thickness as a first indicator of inflammation was strikingly increased in the presence of CD1a (**Fig. 1a**). Histological analysis revealed a pronounced cellular infiltrate especially in the dermis of urushiol-treated CD1aTg animals (**Fig. 1b**). Subsequently, we analyzed the skin-infiltrating cells by flow cytometry and found a significant increase in inflammatory granulocytes and macrophages in CD1aTg mice (**Fig. 1c,d**). Dermal T lymphocytes bearing a γδ T cell receptor (TCR) expanded to the same extent in both mouse strains (**Fig. 1e,f**). By contrast, the presence of CD1a promoted the specific amplification of CD4 αβ T cells, whereas the participation of CD8 T cells proved to be negligible (**Fig. 1e,f**). Investigating the functional cytokine responses of these lymphocytes, we found that the abundance of CD4 T cells producing IL-17 and IL-22 (Th17 cells) was drastically increased in the CD1aTg mouse model (**Fig. 1g,h**). Thus, CD1a promotes Th17-mediated skin inflammation in response to poison ivy. Next, we investigated whether our findings in the mouse model were relevant in humans. For this purpose, we tested memory T cells from the blood of human subjects who experienced moderate-to-severe poison ivy rash in the past six months. CD1a-transfectant antigen-presenting cells or parental control cells were pulsed with urushiol or vehicle, prior to coculture with T lymphocytes from poison ivy or healthy donors. Subsequent analysis of T cell activation revealed increased IL-17- and IL-22 production of T cells from

poison ivy donors that specifically responded to urushiol in a CD1a-dependent manner (**Fig. 2a,b**). Thus, in the context of our data in the CD1a-transgenic system, human subjects with poison ivy dermatitis showed a similar inflammatory cytokine signature following CD1a-mediated urushiol recognition.

Adaptive immunity to poison ivy is distinct from a classical hapten response

Next, we determined whether the immune response to urushiol was based on adaptive immunity, or innate mechanisms locally at work in the skin. In the absence of initial sensitization, CD1aTg mice that were only challenged with urushiol failed to develop increased skin inflammation, as indicated by skin infiltration and IL-17-producing CD4 T cells (**Fig 3a,b**). Although urushiol showed a direct impact on innate inflammation, upregulation of inflammatory mediators, such as IL-1β and TNF-α, was comparable between CD1aTg and wild-type mice (**Supplementary Fig. 1**). Therefore, CD1a-dependent immunity to urushiol involves antigen-specific T cell priming. To exclude a generally increased susceptibility of CD1aTg mice to antigenic stimulation, we tested the immune response to the classical hapten dinitrofluorobenzene (DNFB)[23]. Surprisingly, ear swelling was reduced in the CD1aTg mouse model when compared to wild-type (**Supplementary Fig. 2a**). In addition to reduced influx of inflammatory granulocytes, CD1aTg mice generated drastically less CD8 T cells in response to DNFB and accordingly showed reduced IFN-γ production (**Supplementary Fig. 2b,c**). Thus, the CD1aTg mice do not have a generally increased susceptibility to stimulation with hapten.

CD1a on Langerhans cells is important for generation of Th17 cells and dermatitis

Using confocal microscopy of epidermal sheets, we demonstrate the Langerhans cell network in the epidermis as well as their exclusive CD1a expression in the CD1aTg mouse model (**Fig. 4a**). Moreover, we analyzed all skin DCs by flow cytometry and found the CD1a-positive population

to super-impose with langerin-expressing Langerhans cells (**Fig. 4b**). Subsequently, we monitored CD1a expression on skin DCs during the immune response to urushiol. In vehicle-treated control skin, the composition of skin DCs proved to be comparable between CD1aTg and wild-type mice, indicating normal homeostasis (**Fig. 4c**). In the inflamed ear skin, we observed a massive influx of inflammatory, CD1a-negative DCs. By contrast, epidermal Langerhans cells were the main population specifically expressing CD1a in poison ivy dermatitis (**Fig. 4c**). Based on this exclusive expression pattern, we next aimed at inhibiting CD1a function on Langerhans cells. For this purpose, we treated mice during the sensitization phase with CD1a blocking antibodies. Strikingly, anti-CD1a treatment reduced ear swelling in CD1aTg animals to wild-type levels as compared to administration of isotype control antibodies (**Fig. 4d**). Accordingly, infiltration of inflammatory granulocytes and IL-17-producing CD4 T cells was equally abrogated by anti-CD1a treatment (**Fig. 4e,f**). Of note, antibody application had no depletional effect but rather blocked CD1a function on the surface of Langerhans cells. In this context, we found downregulation of CD1a on skin Langerhans cells upon antibody treatment, although diminishment of CD1a appeared incomplete possibly due to limited accessibility of the epidermis for systemically administered antibodies **(Fig. 4g**). However, in skin-draining lymph nodes, anti-CD1a treatment led to full downregulation of CD1a on migrating Langerhans cells (**Fig. 4g**). Taken together, CD1a-expressing Langerhans cells are essential for generation of Th17 cells and skin inflammation.

Urushiol (C15:2) is the dominant antigen for CD1a-restricted T cells

Since poison ivy induced strong CD1a-mediated inflammation, we next investigated whether urushiol is a bona fide antigen presented by CD1a. For this purpose, we incubated plate-bound recombinant human CD1a molecules with urushiol, prior to culture with CD4 T cells isolated

from urushiol-immunized mice. In sharp contrast to lymphocytes from wild-type mice, only CD4 T cells isolated from CD1aTg animals produced IL-17 in response to urushiol-loaded CD1a molecules (**Fig. 5a**). This system is free of antigen-presenting cells and thus demonstrates the direct presentation of urushiol by CD1a. Since natural urushiol contains a mixture of different pentadecylcatechols, we subsequently determined which congener of poison ivy was responsible for its antigenic properties. Using the same recombinant CD1a system, we found that pentadecylcatechol with two unsaturations (C15:2) is the dominant immunogen for CD1a-mediated T cell activation (**Fig. 5b**). We also showed that C15:2 mediated the observed effects of increased skin inflammation in CD1aTg mice (**Fig. 5c**). In order to mimic urushiol presentation in its natural habitat, we isolated Langerhans cells from ear skin of immunized CD1aTg animals, prior to pulsing with C15:2 and coculture with CD4 T cells from draining lymph nodes. Langerhans cells triggered a strong Th17 cell response upon C15:2 presentation in a strictly CD1a-specific manner, because anti-CD1a fully abolished T cell activation (**Fig. 5d**). Of note, a substantial degree of autoreactive, CD1a-restricted T cell stimulation could be observed with unpulsed Langerhans cells (**Fig. 5d**). A classical feature of adaptive immunity is the clonal expansion of antigen-specific T cells, characterized by a certain TCR usage of amplified cells. Therefore, we investigated the TCR repertoire of the immune response to urushiol. Notably, T cells exhibited a significant increase in Vβ2 and Vβ4 TCR usage in inflamed skin of CD1aTg mice, suggesting clonal expansion under antigenic selection pressure (**Supplementary Fig. 3a**). The $V\beta2^+$ and $V\beta4^+$ T cell clones produced higher amounts of IL-17 in CD1aTg animals compared to wild-type mice (**Supplementary Fig. 3b**). Moreover, amplification of $V\beta2^+$ and $V\beta4^+$ T cells was significantly hampered when CD1a function was blocked by antibody treatment (**Supplementary Fig. 3c**). These changes in TCR repertoire were

specific for T cells in skin inflammation, because normal control skin showed no difference in TCR usage between wild-type and CD1aTg mice (**Supplementary Fig. 3d**). Additionally, the CD1aTg mouse model revealed no alterations of the TCR repertoire in the thymus, excluding differential thymic selection (**Supplementary Fig. 3e**). Altogether, our results on functional presentation and TCR repertoire suggest that urushiol is an antigen for CD1a-restricted T cells.

Crystal structure of the CD1a-urushiol (C15:2) complex

Therefore, we aimed to obtain molecular insight into the mechanism of CD1a presenting urushiol. To establish this, we recombinantly expressed the CD1a molecule in mammalian cells and in vitro loaded the urushiol ligand (C15:2). As CD1a expressed in mammalian cells comprises a heterogeneous array of self lipid ligands within its antigen-binding cleft, the endogenous lipids were initially displaced by the ganglioside GD_3. Subsequently, GD_3 bound to CD1a was specifically displaced by urushiol, with the CD1a-urushiol complex being purified from CD1a-GD_3 via anion-exchange chromatography. Next, we crystallized and determined the structure of the CD1a-urushiol binary complex to 1.9Å resolution (**Fig. 6a** and **Supplementary Table 1**). Unbiased electron density was visible for the urushiol ligand, with the ligand clearly being non-covalently bound within the CD1a antigen-binding cleft (**Supplementary Fig. 4**). Mass spectrometry analysis confirmed the presence of urushiol (m/z 317.24) both in the purified recombinant CD1a sample loaded with urushiol and in crystals of the CD1a-urushiol binary complex (**Fig. 6b,c**). Accordingly, CD1a directly presents urushiol.

The antigen-binding cleft of CD1a comprises the A'- and F'-pockets, in which the A'-pocket is considered to function as a molecular ruler, favoring acyl chains between C_{18}-$_{20}$ in length[14]. For example, in the structure of the CD1a-lysophosphatidylcholine complex, the acyl chain winds round the A'-pocket while the polar headgroup is positioned at the junction of A'- and F'-

portals[15]. As anticipated, the urushiol antigen is positioned deep in the CD1a binding cleft, spanning from the A'- to the F'-pocket (**Supplementary Fig. 4a**). Surprisingly however, the catechol headgroup and acyl chain were positioned towards the A'- and F-pockets, respectively, in the reverse direction to what may have been anticipated based on previous CD1a-antigen structures (**Fig. 6a**, right panel)[4]. Here, the urushiol antigen mainly interacted via van der Waals contacts with residues of the α1-helix of CD1a (**Fig. 6a** and **Supplementary Table 2**). The aromatic catechol headgroup of the antigen was positioned in the A'-pocket and stacked against Phe70, while the 3'-hydroxyl formed a hydrogen bond with the main chain carbonyl of Leu66. The C15:2 aliphatic tail of urushiol sat over the hydrophobic platform formed by Val12, Trp14, Val98, and Leu116 (**Fig. 6a**). 80% of the urushiol molecule is buried within the CD1a cleft (Buried Surface Area of ~495 $Å^2$). Thus, CD1a presents the urushiol antigen with 20% of its molecular surface potentially exposed at the F'-portal for direct TCR contact (**Supplementary Fig. 4b**).

CD1a facilitates psoriatic skin inflammation dominated by Th17 cells

Based on the substantial IL-17 production by CD1a-autoreactive T cells (**Fig. 5d**) and the prominent function of IL-17 in psoriasis[24,25], we hypothesized that CD1a might play an important role in psoriatic inflammation. Therefore, we investigated CD1aTg mice in a well-established model for psoriasiform inflammation, using skin administration of the small molecule compound imiquimod[29]. Histological analysis revealed strong cellular infiltration of the skin and dramatic epidermal hyperplasia in CD1aTg mice when compared to controls (**Fig. 7a**). Histopathology was reflected in the macroscopic, psoriasis-like aspect of ear skin that exhibited swelling, reddening, and scaling (**Fig. 7a,b**). Next, we aimed at therapy of psoriasiform inflammation using CD1a blocking antibodies. Strikingly, anti-CD1a treatment significantly reduced skin

inflammation in CD1aTg animals (**Fig. 7c**). This therapeutic effect was mirrored by reduction of inflammatory granulocytes and CD4 T cells that produced IL-17A, IL-17F, and IL-22 (**Fig. 7d,e**). Taking into account that we did not challenge CD1aTg mice with exogenous lipids in this psoriasis model, we hypothesized that during the inflammatory process, self lipid antigens are released to facilitate CD1a-mediated T cell responses and skin inflammation. To this end, we isolated T cells from skin-draining lymph nodes of imiquimod-treated mice, prior to incubation with plate-bound CD1a molecules loaded with self lipids that have been previously reported as skin antigens[9]. T cells from CD1aTg mice specifically responded to CD1a-restricted self lipid presentation, with pronounced recognition of fatty acid and triacylglycerol (**Fig. 7f**). Of note, we could not detect any meaningful production of IL-17 in untreated controls, underscoring that in the absence of inflammation, there is a complete lack of self lipid antigen presentation and recognition (**Fig. 7f**). Ultimately, we wanted to translate our findings in the psoriasis-like model to the human system. For this purpose, we studied a cohort of patients with moderate-to-severe plaque psoriasis compared to healthy donors, measuring CD1a-restricted T cell activation. Accordingly, memory T cells from the blood of psoriasis patients or healthy donors were stimulated with autologous monocyte-derived DCs in the presence or absence of anti-CD1a, prior to measurement of cytokine responses. Notably, we observed an increase in protein production of IL-17 and IL-22 in T cells from psoriasis patients when compared to healthy controls (**Fig. 7g**). Moreover, the inflammatory cytokine response from patients was significantly blocked by anti-CD1a treatment (**Fig. 7g**). Taken mouse model for psoriasis and human studies together, we present strong evidence that CD1a drives psoriatic skin inflammation and that targeting CD1a can abrogate inflammatory skin disease.

DISCUSSION

Using the CD1a-transgenic model, our studies demonstrate a vital role for CD1a in skin inflammation in vivo. Since wild-type mice lack CD1a expression, previous reports investigating Langerhans cell functions in the murine system neglect the integral role of CD1a. Therefore, our new model is able to demonstrate the entire spectrum of Langerhans cell abilities, including CD1a as their prominent hallmark molecule. We show that poison ivy-induced skin inflammation is dominated by CD1a-dependent Th17 cells. Using wild-type mice in the absence of CD1a, previous work suggested CD8 T cells and IFN-γ to respond to urushiol[30]. However, the magnitude of inflammation appeared to be relatively mild[30], which is in agreement with our observations in control animals. In sharp contrast, the response to poison ivy is much stronger in humans, including skin reddening, blistering, and vigorous itch – a severity well reflected in the CD1a-transgenic mouse model. Urushiol is commonly considered as pro-hapten, whose catechol group is oxidized to a quinone that subsequently reacts with endogenous proteins to form an immunogen[23]. Normally, contact hypersensitivity to haptens is driven by CD8 T cells producing IFN-γ, as seen in response to DNFB and drug hypersensitivities[23,31]. By contrast, we demonstrate urushiol-specific, CD1a-restricted activation of CD4 T cells that secrete IL-17. Moreover, immune stimulation by DNFB was suppressed in CD1aTg mice, indicating that CD1a does not favor hapten responses.

Based on presentation experiments using recombinant CD1a or Langerhans cells, and our structural studies on the CD1a-urushiol complex, we demonstrate that urushiol (C15:2) is a veritable antigen for CD1a-restricted T cells. While the overall structural features of the CD1a binding cleft were generally conserved upon urushiol binding by comparison to the previous CD1a-antigen complexes[15], two CD1a residues deep within the A'-pocket underwent structural

rearrangements in order to accommodate the urushiol antigen in the binding groove. Namely, Phe70 and Trp14 swung away to provide space for the catechol headgroup and the C15-tail of urushiol, respectively (**Fig. 6a**). These conformational changes had the knock-on effect of altering the conformation of the CD1a antigen-binding cleft (root mean square deviation of 0.6 Å), in particular residues 146-150 (r.m.s.d. of 1.3 Å), which subsequently impacted on the conformation of Arg73, Arg76, and Glu154 (**Fig. 6a**), a constellation of residues known to impact on the autoreactivity of a CD1a-restricted TCR[15]. Thus, a region of the urushiol antigen is accessible for direct TCR contact within the CD1a groove (**Supplementary Fig. 4b**), and moreover, the accommodation of urushiol leads to conformational changes within CD1a that could also directly impact on TCR recognition. However, future studies will be required to show the ternary structure of CD1a-urushiol-TCR.

Furthermore, we demonstrated that CD1a on Langerhans cells controls inflammation in psoriasis, exploring a psoriasis-like mouse model as well as patients. Considering our findings on presentation of fatty acid and triacylglycerol, we propose that self lipids could represent dominant antigens in psoriasis when displayed by CD1a. A recent study revealed that self lipids fitting into the CD1a binding groove can change the conformation of CD1a to be recognized by specific TCRs, in a mechanism of permissive autoreactivity[15]. Integrating follow-up human studies using patient samples, the concept of self lipids might provide important answers to the long quest for antigens so far unknown in psoriasis. The skin harbors a multitude of immune cells involved in the response to challenges. Dermal γδ T cells produce IL-17 and have been associated with psoriasis[32,33]. We observed a comparable increase of dermal γδ T cells in CD1aTg or wild-type mice in response to urushiol or imiquimod. By contrast, amplification of IL-17-producing αβ T cells was specific for the CD1aTg model, thus explaining the predominant

impact of CD1a-dependent Th17 cells on skin inflammation. Yet, both T cell populations can complement each other, with γδ T cells responding early and in an innate fashion to cytokines such as IL-23, and CD1a-restricted Th17 cells acting at a later stage in a lipid antigen-specific manner. In psoriasis patients, we found a particular increase in inflammatory IL-17 and IL-22 production upon recognition of CD1a. Finally, our results demonstrate that blocking CD1a in vivo using antibody treatment is able to substantially reduce skin inflammation. Thus, we propose targeting of CD1a to pave the way for future CD1a-based therapies against inflammatory skin diseases.

REFERENCES

1. Brigl, M. & Brenner, M.B. CD1: antigen presentation and T cell function. *Annu. Rev. Immunol.* **22**, 817-890 (2004).

2. Porcelli, S. *et al.* Recognition of cluster of differentiation 1 antigens by human CD4-CD8-cytolytic T lymphocytes. *Nature* **341**, 447-450 (1989).

3. Kain, L. *et al.* The identification of the endogenous ligands of natural killer T cells reveals the presence of mammalian alpha-linked glycosylceramides. *Immunity* **41**, 543-554 (2014).

4. Van Rhijn, I., Godfrey, D.I., Rossjohn, J. & Moody, D.B. Lipid and small-molecule display by CD1 and MR1. *Nat. Rev. Immunol.* **15**, 643-654 (2015).

5. Agea, E. *et al.* Human CD1-restricted T cell recognition of lipids from pollens. *J. Exp. Med.* **202**, 295-308 (2005).

6. Pena-Cruz, V., Ito, S., Dascher, C.C., Brenner, M.B. & Sugita, M. Epidermal Langerhans cells efficiently mediate CD1a-dependent presentation of microbial lipid antigens to T cells. *J Invest Dermatol* **121**, 517-521 (2003).

7. Hunger, R.E. *et al.* Langerhans cells utilize CD1a and langerin to efficiently present nonpeptide antigens to T cells. *J. Clin. Invest.* **113**, 701-708 (2004).

8. Moody, D.B. *et al.* T cell activation by lipopeptide antigens. *Science* **303**, 527-531 (2004).

9. de Jong, A. *et al.* CD1a-autoreactive T cells recognize natural skin oils that function as headless antigens. *Nat. Immunol.* **15**, 177-185 (2014).

10. de Jong, A. *et al.* CD1a-autoreactive T cells are a normal component of the human alphabeta T cell repertoire. *Nat. Immunol.* **11**, 1102-1109 (2010).

11. de Lalla, C. *et al.* High-frequency and adaptive-like dynamics of human CD1 self-reactive T cells. *Eur. J. Immunol.* **41**, 602-610 (2011).

12. Jarrett, R. *et al.* Filaggrin inhibits generation of CD1a neolipid antigens by house dust mite-derived phospholipase. *Sci Transl Med* **8**, 325ra318 (2016).

13. Bourgeois, E.A. *et al.* Bee venom processes human skin lipids for presentation by CD1a. *J. Exp. Med.* **212**, 149-163 (2015).

14. Zajonc, D.M., Elsliger, M.A., Teyton, L. & Wilson, I.A. Crystal structure of CD1a in complex with a sulfatide self antigen at a resolution of 2.15 A. *Nat. Immunol.* **4**, 808-815 (2003).

15. Birkinshaw, R.W. *et al.* alphabeta T cell antigen receptor recognition of CD1a presenting self lipid ligands. *Nat. Immunol.* **16**, 258-266 (2015).

16. Gomez Perdiguero, E. *et al.* Tissue-resident macrophages originate from yolk-sac-derived erythro-myeloid progenitors. *Nature* **518**, 547-551 (2015).

17. Hoeffel, G. *et al.* Adult Langerhans cells derive predominantly from embryonic fetal liver monocytes with a minor contribution of yolk sac-derived macrophages. *J. Exp. Med.* **209**, 1167-1181 (2012).

18. Wang, Y. *et al.* IL-34 is a tissue-restricted ligand of CSF1R required for the development of Langerhans cells and microglia. *Nat. Immunol.* **13**, 753-760 (2012).

19. Igyarto, B.Z. & Kaplan, D.H. Antigen presentation by Langerhans cells. *Curr. Opin. Immunol.* **25**, 115-119 (2013).

20. Merad, M., Ginhoux, F. & Collin, M. Origin, homeostasis and function of Langerhans cells and other langerin-expressing dendritic cells. *Nat. Rev. Immunol.* **8**, 935-947 (2008).

21. Bobr, A. *et al.* Acute ablation of Langerhans cells enhances skin immune responses. *J. Immunol.* **185**, 4724-4728 (2010).

22. Igyarto, B.Z. *et al.* Skin-resident murine dendritic cell subsets promote distinct and opposing antigen-specific T helper cell responses. *Immunity* **35**, 260-272 (2011).

23. Kaplan, D.H., Igyarto, B.Z. & Gaspari, A.A. Early immune events in the induction of allergic contact dermatitis. *Nat. Rev. Immunol.* **12**, 114-124 (2012).

24. Lowes, M.A., Bowcock, A.M. & Krueger, J.G. Pathogenesis and therapy of psoriasis. *Nature* **445**, 866-873 (2007).

25. Perera, G.K., Di Meglio, P. & Nestle, F.O. Psoriasis. *Annu Rev Pathol* **7**, 385-422 (2012).

26. Kalish, R.S. The use of human T-lymphocyte clones to study T-cell function in allergic contact dermatitis to urushiol. *J Invest Dermatol* **94**, 108S-111S (1990).

27. Kalish, R.S. & Johnson, K.L. Enrichment and function of urushiol (poison ivy)-specific T lymphocytes in lesions of allergic contact dermatitis to urushiol. *J. Immunol.* **145**, 3706-3713 (1990).

28. Kalish, R.S., Wood, J.A. & LaPorte, A. Processing of urushiol (poison ivy) hapten by both endogenous and exogenous pathways for presentation to T cells in vitro. *J. Clin. Invest.* **93**, 2039-2047 (1994).

29. van der Fits, L. *et al.* Imiquimod-induced psoriasis-like skin inflammation in mice is mediated via the IL-23/IL-17 axis. *J. Immunol.* **182**, 5836-5845 (2009).

30. Wakabayashi, T. *et al.* IFN-gamma and TNF-alpha are involved in urushiol-induced contact hypersensitivity in mice. *Immunol. Cell Biol.* **83**, 18-24 (2005).

31. Illing, P.T. *et al.* Immune self-reactivity triggered by drug-modified HLA-peptide repertoire. *Nature* **486**, 554-558 (2012).

32. Cai, Y. *et al.* Pivotal role of dermal IL-17-producing gammadelta T cells in skin inflammation. *Immunity* **35**, 596-610 (2011).

33. Gray, E.E., Suzuki, K. & Cyster, J.G. Cutting edge: Identification of a motile IL-17-producing gammadelta T cell population in the dermis. *J. Immunol.* **186**, 6091-6095 (2011).

Supplementary Information is available in the online version of the paper.

Acknowledgements We thank M. Brenner for providing CD1a antibody, B. Moody and T.-Y. Cheng for providing K562 cells and advice regarding human T cell assays. We are grateful to A. Del Grosso for sharing natural urushiols. We thank J. Ordovas-Montanes for advice regarding preparation of skin tissue. We thank the NIH tetramer facility for providing CD1a-monomers. We thank the staff at the Australian synchrotron for assistance with data collection. J.H.K. was supported by the National Research Foundation of Korea (2012R1A6A3A03040248) and the AMOREPACIFIC Research Scholar Program. J.R. was supported by an NHMRC Australia Fellowship. This work was supported by the NHMRC and the ARC (J.R.), and NIH grant R01 AI083426 (F.W.).

Author Contributions J.H.K. and Y.H. designed and performed experiments, and wrote the manuscript. T.Y. performed crystallography and structural analysis. Q.W. and J.K. performed flow cytometry and helped revise the manuscript. V.A.H., J.L.N., E.A.M., and A.W.P. performed HPLC, mass spectrometry, crystallography, and analyzed data. M.S. generated human CD1a-transgenic mice. J.R. and F.W. designed and supervised experiments, and wrote the manuscript.

Author Information The authors declare no competing financial interest.

Correspondence and requests for materials should be addressed to J.R. (jamie.rossjohn@monash.edu) or F.W. (florian.winau@childrens.harvard.edu)

METHODS

Reagents. RPMI medium 1640, propidium iodide (PI), ethylenediaminetetraacetic acid (EDTA), β-mercaptoethanol, penicillin and streptomycin, sodium pyruvate, and L-glutamine were purchased from Life Technologies. Fetal bovine serum (FBS), bovine serum albumin (BSA), and phosphate-buffered saline (PBS) were from Sigma-Aldrich. RPMI medium 1640 was supplemented with 10% FBS, penicillin and streptomycin (10 U/ml), sodium pyruvate (1 mM), L-glutamine (2 mM), β-mercaptoethanol (50 μM), and HEPES (100 mM). Purified natural urushiol was a generous gift from Alfred Del Grosso at the Food and Drug Administration (FDA). Synthetic urushiols C15:1, C15:2, and C15:3 were purchased from Phytolab (Germany). Synthetic urushiol C15:0 was obtained from ChromaDex. Palmitoleic acid, squalene, and glyceryl tripalmitoleate were purchased from Sigma-Aldrich. Oleyl palmitoleate and oleyl oleate were from Nu-Chek.

Antibodies. For flow cytometry, cells were stained with following antibodies: anti-CD3ε (145-2C11), anti-CD8α (53-6.7), anti-CD4 (GK1.5), anti-CD45.2 (104), anti-IFN-γ (XMG1.2), anti-CD1a (HI149), anti-IL-17F (9D3.1C8), anti-IL-22 (Poly5164), anti-γδTCR (GL3), anti-CD11b (M170), anti-Gr-1 (RB6-8C5), anti-F4/80 (BM8), anti-CD11c (N418), and anti-CD11a (M17/4) were purchased from BioLegend. Anti-IL-17A (ebio17B7), anti-CD207 (eBioL31), anti-CD103 (2E7), anti-RORγt (B2D), and anti-MHC class II (M5/114.15.2) were from eBioscience. Anti-CD1a antibody (10H3) for blocking was kindly provided by Michael Brenner at Brigham and Women's Hospital. Anti-CD16/CD32 (2.4G2) was acquired from Bio-XCell. Secondary antibodies anti-mouse IgG and anti-rat IgG were from Life Technologies. To study the repertoire of Vβ TCRs, the Mouse Vβ TCR Screening Panel (BD Pharmingen) was used.

Mice and models of skin inflammation. Human CD1a-transgenic mice were generated as previously reported[34]. C57BL/6 and OT-II transgenic mice were purchased from The Jackson Laboratory. Sex- and age-matched animals between 8 and 12 weeks of age were used for experiments. Preliminary experiments were performed to determine proper sample size. All animal experiments were approved by the Institutional Animal Care and Use Committee (IACUC) of Harvard Medical School. For triggering skin inflammation, mice were sensitized on the shaved abdomen with 30 μl of 20 mg/ml urushiol, or 0.5% DNFB (Sigma) dissolved in acetone (Sigma). Five days after sensitization, mice were challenged on dorsal and ventral side of the ear with 10 μl of 5 mg/ml urushiol or 0.2% DNFB. To induce psoriatic skin inflammation, 5% imiquimod cream (Glenmark) was topically applied on dorsal and ventral sides of ears for 6-7 consecutive days as previously described[35]. Ear thickness was measured before and after treatment using a micrometer (Swiss Precision Instruments). To block CD1a-dependent responses, mice were injected with 100 μg of anti-CD1a or isotype control antibody at -3, -1, +1, +3, +5 days before and after treatment.

Mouse tissue preparation. Ears were excised, split into two halves at an angle parallel to the cartilage, and further cut into small pieces. Tissue samples were digested in RPMI containing 0.1 mg/ml Liberase TM (Roche Diagnostic Corp.), 0.1 mg/ml DNase I (Roche Diagnostic Corp.), and 20 μM HEPES (Life Technologies) for 2 hours at 37°C with shaking (140 rpm). Digested samples were minced through a metal mesh, and filtered with a 70 μm nylon strainer (BD Biosciences). Auricular lymph nodes and thymi were harvested and minced through a metal mesh to obtain single cell suspensions. To isolate CD4 T cells, cell suspensions were incubated

with anti-CD16/CD32 for 10 minutes on ice, and CD4-positive cells were selected using CD4 magnetic beads and MACS columns (Miltenyi Biotec) according to manufacturer's protocol.

Langerhans cell isolation. Langerhans cells (LCs) from ear skin were isolated as previously described[36]. Briefly, ears were split into dorsal and ventral halves, and incubated in 0.8% trypsin solution (Sigma-Aldrich) for 25-45 minutes at 37°C. Epidermal layers were peeled off from the dermis and transferred into complete RPMI medium, followed by stirring for 40 minutes at 37°C in a water bath incubator (Labline Instruments). Cell suspensions were passed through 70 μm nylon strainers. To remove dead cells, a gradient centrifugation with Percoll (GE Healthcare) was performed. Cells were stained with anti-CD11c magnetic beads, and CD11c-positive cells were sorted by MACS columns. Approximately 70% of isolated cells were $CD1a^{+}$MHC class II^{+} LCs.

T cell assay with LCs. LCs were pulsed with 5 μg/ml urushiol or vehicle in complete media for 2 hours, and subsequently co-cultured with T cells at a ratio of 1:5 in 96-well round-bottom plates. To block CD1a-dependent responses, LCs were incubated with 10 μg/ml anti-CD1a (10H3) or isotype control antibody for 2 hours, prior to the addition of T cells. After 3 days, culture supernatants were harvested to perform ELISA for IL-17A and IFN-γ.

T cell experiments with plate-bound recombinant CD1a. Biotinylated CD1a monomers paired with β_2-microglobulin (β2M) were provided by the NIH Tetramer Facility. CD1a-coated plates and lipid antigens were prepared as described previously[9]. Briefly, streptavidin-coated plates (Thermo Scientific) were incubated with biotinylated human CD1a-β2M monomers (1

μg/well) and anti-CD11a (0.25 μg/ml) in PBS for 18 hours at room temperature. After washing with PBS, the plates were incubated with citrate buffer (pH 3.4) for 20 minutes, repeated twice with three washing steps in between. Lipid antigens were dissolved in PBS containing 0.05% Tween 20 (1-100 μM) by sonication for 30 minutes at room temperature in a water bath sonicator (Branson), followed by heating at 56°C for 20 minutes, prior to addition to plates coated with CD1a. After 48 hours of incubation at room temperature, the plates were washed with PBS three times. T cells suspended in complete media were added to the plates ($1\text{-}2x10^4$ skin CD4 T cells, or $1x10^5$ lymph node CD4 T cells per well), and cultured for 3-5 days at 37°C in a CO_2 incubator (Thermo Scientific). Culture supernatants were used for cytokine analysis by ELISA.

Human T cell assays. For the psoriasis study, patients diagnosed with moderate-to-severe plaque psoriasis were included in the study based on their Psoriasis Area Severity Index (PASI). The PASI integrates criteria including erythema, induration, desquamation, and percentage of affected skin area. Monocyte-derived CD1a-expressing dendritic cells (mDCs) and memory CD4 T cells were prepared as previously described[10]. mDCs were treated with LPS (100 ng/ml) for 3 hours, prior to coculture with CD4 T cells. After expansion for 10 days, T cells were tested for CD1a auto-reactivity by co-culture with autologous mDCs at a ratio of 1:5 for 3 days in the presence of 10 μg/ml anti-CD1a or isotype control. To test urushiol-specific T cell responses in humans, memory T cells isolated from peripheral blood mononuclear cells (PBMCs) of subjects who had poison ivy dermatitis in the last 6 months or control donors were expanded with autologous DCs pulsed with 2 μg/ml urushiol C15:2 for 10 days. Human IL-2 was added every 3 days during cell culture. Subsequently, urushiol-specific T cell responses were determined by co-

culture of expanded T cells with urushiol C15:2- or vehicle-pulsed CD1a- or mock-transfected K562 cells at a ratio of 1:5. Three days after co-incubation, cells were used for intracellular cytokine staining and analyzed by flow cytometry, and culture supernatants were used for cytokine analysis by ELISA. K562 cells were routinely tested for mycoplasma contamination, and CD1a expression of transfectants was confirmed before use by flow cytometry. PBMCs were obtained from ConversantBio, ALLCELLS, and the Kraft Family Blood Donor Center at Brigham and Women's Hospital. Informed consent was obtained from all subjects, and all human studies were approved by Boston Children's Hospital's Institutional Review Board (IRB).

Flow cytometry and intracellular staining for cytokines. Cells were stained with antibodies against surface antigens in FACS buffer (PBS supplemented with 0.5% BSA) on ice for 30 minutes. Subsequently, cells were washed and analyzed using a FACSCanto™ II flow cytometer (BD Biosciences). Propidium iodide or viability dye (eBioscience) was used to exclude dead cells. For intracellular cytokine staining, cells were stimulated *ex vivo* with 50 ng/ml phorbol myristate acetate (Sigma), and 5 μg/ml ionomycin (Sigma) in the presence of brefeldin A (BioLegend) in complete media for 4 hours at 37°C in a CO_2 incubator. After surface staining, cells were fixed and permeabilized with BD Cytofix/Cytoperm solution followed by staining with antibodies against cytokines in Perm/Wash buffer (BD Biosciences).

RNA extraction and real-time qPCR. Total RNA was purified from ear cells using the RNeasy Plus Mini Kit (Qiagen) according to the manufacturer's instructions. RNA was converted to cDNA with High Capacity *RNA*-to-*cDNA* Kit (Applied Biosystems). cDNA was mixed with primers and iTaq universal *SYBR Green* supermix (Bio-Rad), and relative expression was

determined by real-time PCR using a 7300 Real-Time PCR System (Applied Biosystems). β-actin was used as a housekeeping control. To calculate the relative fold change, the $2^{-\Delta\Delta CT}$ cycle threshold method was used. The following primer sequences were used:

Actb, forward, 5'-TCCAGCCTTCCTTCTTGGGTATGGA-3',

Actb, reverse, 5'-CGCAGCTCAGTAACAGTCCGCC-3',

Il1b, forward, 5'-CAGGCAGGCAGTATCACTCA-3',

Il1b, reverse, 5'-AGGTGCTCATGTCCTCATCC-3',

Il22, forward, 5'-CCGAGGAGTCAGTGCTAAGG-3',

Il22, reverse, 5'-GTAGGGCTGGAACCTGTCTG-3',

Tnfa, forward, 5'-CCGATGGGTTGTACCTTGTC-3',

Tnfa, reverse, 5'-AGATAGCAAATCGGCTGACG-3',

Il23, forward, 5'-CCAGCGGGACATATGAATCT-3',

Il23, reverse, 5'-TGTGGGTCACAACCATCTTC-3',

Il10, forward, 5'-CCAAGCCTTATCGGAAATGA-3',

Il10, reverse, 5'-TCTCACCCAGGGAATTCAAA-3',

Il17A, forward, 5'-AGCTGGACCACCACATGAAT-3',

Il17A, reverse, 5'-AGCATCTTCTCGACCCTGAA-3',

Human *Il22*, forward, 5'-GCTTGACAAGTCCAACTTCCA-3',

Human *Il22*, reverse, 5'-GCTCACTCATACTGACTCCGT-3',

Human *Il17A*, forward, 5'-TCCCACGAAATCCAGGATGC-3',

Human *Il17A*, reverse, 5'-GGATGTTCAGGTTGACCATCAC-3',

Human *Ifng*, forward, 5'-TCGGTAACTGACTTGAATGTCCA-3',

Human *Ifng*, reverse, 5'-TCCTTTTTCGCTTCCCTGTTTT-3'.

Histology and confocal microscopy. Mice were euthanized by CO_2 inhalation, and ear samples were frozen in Optimal Cutting Temperature (OCT) compound (Sakura Finetechnical Corporation). Ten μm-thick cross-sections were made and stained with hematoxylin and eosin by the Histology Core at Beth Israel Deaconess Medical Center. Images were taken using a BX63 Motorized Microscope (Olympus). For epidermal sheets, ear pinnae were treated with shaving cream (SoftSheen-Carson) and affixed to slides with the epidermis downward. The ear samples were incubated in 10 mM EDTA in PBS for 2 hours at 37ºC, followed by physical removal of the dermis. Tissue was fixed in 4% paraformaldehyde (Sigma) at room temperature for 30 minutes, and blocked with 10% FBS and 2% goat serum (Life Technologies) in PBS. Tissues were stained with purified anti-MHC class II and anti-CD1a, followed by staining with Alexa Fluor 647-conjugated anti-rat IgG, and Alexa Fluor 488-conjugated anti-mouse IgG as secondary antibodies. Samples were mounted with ProLong® Gold Antifade Mountant including DAPI (Life Technologies). Immunofluorescent images were taken using an Olympus FV1000 confocal microscope.

Expression, purification of CD1a and urushiol (C15:2) loading into CD1a. The glycoprotein CD1a was expressed in a mammalian expression system and purified as previously described[15]. Following an endoglycosidase H (New England BioLabs) treatment, the purified CD1a was first loaded with the ganglioside GD_3 (GD_3) (Matreya LLC) that was dissolved in a solution containing 0.5% tyloxapol (Sigma) and 10 mM Tris buffer at pH 8.0. CD1a was first incubated with GD_3 overnight at room temperature at a molar ratio of 1:15. The CD1a sample loaded with GD_3 was further purified using ion exchange chromatography (MonoQ 10/100 GL-GE

Healthcare). Urushiol C15:2 (Chemos) was dissolved in a solution containing 10 mM Tris buffer at pH 8.0 / 0.5% tyloxapol / 50% acetone (Sigma). The GD_3–CD1a sample was then incubated overnight with urushiol at a 1:15 molar ratio and at room temperature in order to achieve the GD_3 displacement by urushiol. A subsequent purification step involving ion exchange chromatography (MonoQ 10/100 GL) was performed to remove the excess of urushiol C15:2, GD_3 –CD1a, and detergent.

Crystallization, structure determination and refinement. Seeds obtained from previous binary CD1a-antigen crystals[15] were used to grow crystals of the CD1a-urushiol (C15:2) binary complex in 20-25% PEG 1500 / 10% MMT buffer pH 5-6. The crystals were flash-frozen and data were collected at the MX2 beamline (Australian Synchrotron) to a 1.9Å resolution. All the data were processed with the program MOSFLM and were scaled with the CCP4 suite[37]. Consistent with the mass spectrometry data, the urushiol antigen was clearly evident in the unbiased electron density maps, in addition a trace amount of an endogenous self antigen was also evident on account of the high resolution of the binary complex. An initial run of rigid body refinement was performed with the refinement program BUSTER 2.10[38]. Iterative model improvement with COOT[39] and further refinement with BUSTER 2.10[38] were performed. The final refinement led to an R/R-free (%) of 18.6/21.6. The quality of the structure was confirmed at the Research Collaboratory for Structural Bioinformatics Protein Data Bank Data Validation and Deposition Services website. All presentations of molecular graphics were created with the PyMOL molecular visualization system (The PyMOL Molecular Graphics System, Version 1.5.0.4 Schrödinger, LLC.).

Extraction of urushiol and mass spectrometry analysis. In all samples, urushiol was extracted using a single phase Folch procedure[40] and analyzed using a Q-Exactive Hybrid Quadrupole-Orbitrap. Prior to urushiol extraction, crystals of CD1a-urushiol were extensively washed with the crystallization mother liquor and dissolved in Tris Buffer Saline (TBS), pH 8.0. MS coupled to a RSLC nano HPLC (Thermo Scientific, Bremen, Germany). Samples were loaded onto a nanoviper pepmap100 trap column (100µm x 2cm) in 2% acetonitrile / 0.1% ammonium acetate at a flow rate of 15 µL / minute. Analytes were separated at a flow rate of 300 µL / minute on a pepmap100 C18 column (75µm x 15cm, Thermo Scientific) using a linear gradient of acetonitrile (2-80%). Up to 12 MS/MS spectra were acquired per cycle with maximum accumulation time of 50 ms and 100 ms for MS1 and MS2, respectively. A SCIEX QTRAP 5500 mass spectrometer was used for MRM-based detection as previously described[41]. The 5500 mass spectrometer was operated with unit quadrupole resolution and three MRM transitions were simultaneously monitored in detecting U15 315.2→149.1, 315.2→135.1, 315.2→122.1. Data analysis was performed using a combination of Analyst v1.5.2 and XCalibar 3.0 (Thermo Fisher Scientific).

Statistical analysis. Data are presented as mean ± standard error. No statistical method was used to predetermine sample size, which instead was determined based on the results of preliminary experiments. Mice were allocated at random to experimental groups. Mouse studies were performed in a non-blinded fashion. To compare two groups, the two-tailed unpaired Student's t-test, or Mann-Whitney, or Wilcoxon test was used with or without the assumption of normality, respectively. The variance between groups was similar within each group. To compare more than two groups, one-way ANOVA test was performed with post multiple comparisons. p values >

0.05 were considered not significant. All statistical analysis was calculated using Prism software (GraphPad).

References for Methods

34. Kobayashi, C. *et al.* GM-CSF-independent CD1a expression in epidermal Langerhans cells: evidence from human CD1A genome-transgenic mice. *J Invest Dermatol* **132**, 241-244 (2012).

35. Riol-Blanco, L. *et al.* Nociceptive sensory neurons drive interleukin-23-mediated psoriasiform skin inflammation. *Nature* **510**, 157-161 (2014).

36. Stoitzner, P., Romani, N., McLellan, A.D., Tripp, C.H. & Ebner, S. Isolation of skin dendritic cells from mouse and man. *Methods Mol Biol* **595**, 235-248 (2010).

37. Winn, M.D. *et al.* Overview of the CCP4 suite and current developments. *Acta Crystallogr D Biol Crystallogr* **67**, 235-242 (2011).

38. Bricogne, G. *et al. BUSTER* version 2.10.0 (Cambridge, UK: Global Phasing Ltd). (2011).

39. Emsley, P., Lohkamp, B., Scott, W.G. & Cowtan, K. Features and development of Coot. *Acta Crystallogr D Biol Crystallogr* **66**, 486-501 (2010).

40. Alshehry, Z.H. *et al.* An Efficient Single Phase Method for the Extraction of Plasma Lipids. *Metabolites* **5**, 389-403 (2015).

41. Schittenhelm, R.B., Sian, T.C., Wilmann, P.G., Dudek, N.L. & Purcell, A.W. Revisiting the arthritogenic peptide theory: quantitative not qualitative changes in the peptide repertoire of HLA-B27 allotypes. *Arthritis Rheumatol* **67**, 702-713 (2015).

Figure Legends

Figure 1 CD1a facilitates Th17-mediated skin inflammation caused by poison ivy**.** Mice were sensitized by painting urushiol on the abdomen on day 0, and challenged with either urushiol or vehicle on the ear on day 5. (**a**) Ear swelling after challenge (n=5). * P<0.05, ** P<0.01, using Student's t-test. (**b**) Cross-sections of ears obtained 2 days after challenge were stained with hematoxylin and eosin. E=Epidermis, D=Dermis, C=Cartilage; Scale bar: 100 μm. (**c-h**) Flow cytometry analysis of granulocytes and T cell subsets in ear skin 2 days after challenge. (**c**, **d**) Frequencies of inflammatory granulocytes (Gr-1^{high}CD11b^{high}) and macrophages (F4/80^{+}Gr-1^{+}, or F4/80^{+}Gr-1^{-}). (**e**) Frequencies of αβ and γδ T cells among live CD45^{+} cells. (**f**) Absolute cell numbers of indicated T cell subsets. (**g**, **h**) Frequencies and absolute cell numbers of IFN-γ^{+}, IL-17A^{+}, and IL-22^{+} cells among TCRβ^{+}CD4^{+} cells. Error bars represent s.e.m. Results are representative of 5 independent experiments. Three mice per group were used. * P<0.05, ** P<0.01; N.S., not significant, using Mann-Whitney test.

Figure 2 Human subjects with poison ivy dermatitis show urushiol-specific T cell responses mediated by CD1a. Memory T cells were isolated from donors (n=6) who experienced contact dermatitis caused by poison ivy within the last 6 months, or healthy control donors (n=6), and cocultured with urushiol (C15:2)- or vehicle-loaded CD1a- or mock-transfected K562 cells for 3 days. (**a**) Flow cytometry analysis of IL-17- and IL-22-producing CD4 T cells. (**b**) Frequencies of IL-22^{+} and IL-17A^{+}IL-22^{+} cells among CD4 T cells. Error bars represent s.e.m. * P<0.05, ** P<0.01; N.S., not significant, using Mann-Whitney or Wilcoxon test.

Figure 3 Urushiol-specific T cells are primed during the sensitization phase. Mice were challenged with urushiol on ear skin with or without prior sensitization. (**a**) Ear swelling 2 days after challenge. (**b**) Frequencies of Gr-1^{high}CD11b^{high} granulocytes (left), CD45^{+}TCRβ^{+} cells among live cells (middle), and IL-17A^{+}CD4^{+} cells among TCRβ+ cells (right). Error bars represent s.e.m. Results are representative of 3 independent experiments (n=3 per group for each experiment). ** P<0.01; N.S., not significant, using Student's t-test.

Figure 4 CD1a expression on Langerhans cells is essential for generation of Th17 cells and dermatitis. (**a**) Epidermal sheets were stained for MHC class II and CD1a, prior to analysis by confocal microscopy. Scale bar: 20 μm. (**b**) Cells were isolated from ears of naïve mice and stained for MHC-II, CD11c, CD1a, CD103, and CD207. Left plot presents CD1a expression on live $CD11c^{+}MHC\text{-}II^{hi}$ cells. Right plot shows CD103 and CD207 expression in CD1a-negative (I, green dots) and CD1a-positive (II, red dots) populations of CD1aTg mice gated from the left plot (3 independent experiments). (**c**) Langerhans cell (LC) population was analyzed 2 days after vehicle or urushiol challenge (n=3, 4 independent experiments). $CD11c^{+}MHC\text{-}II^{intermediate}$ (G1), $CD103^{+}CD207^{+}$ (G2a), and $CD103^{-}CD207^{+}$ (G2b) cells among $CD11c^{+}MHC\text{-}II^{hi}$ (G2) cells of urushiol-challenged mice were further analyzed for CD1a expression (far right). (**d**-**g**) Wild-type, CD1aTg, or CD1aTg mice injected with either isotype or anti-CD1a antibody were sensitized and challenged with urushiol (n=3, 4 independent experiments). (**d**) Ear swelling on day 2. Ears and draining lymph nodes (dLN) were harvested and analyzed by flow cytometry for (**e**) frequencies of inflammatory $Gr\text{-}1^{hi}CD11b^{hi}$ granulocytes (top), and $IL\text{-}17A^{+}$ or $IFN\text{-}\gamma^{+}$ cells among $CD45^{+}TCR\beta^{+}CD4^{+}$cells (bottom), (**f**) absolute cell numbers of $CD4^{+}$ T cells (top), and IL-17A-producing $CD4^{+}$ T cells (bottom), and (**g**) CD1a expression on LCs in ear skin and dLN. Error bars represent s.e.m. * P <0.05, ** P <0.01; N.S., not significant, using one-way ANOVA and multiple comparisons.

Figure 5 Urushiol is an antigen for CD1a-restricted T cells. (**a**, **b**) Skin $CD4^{+}$ T cells were isolated on day 2 after urushiol challenge, and (**a**) stimulated by plate-bound CD1a loaded with 50 μM natural urushiol (n=3, 5 independent experiments), or (**b**) various concentrations (10, 50, 100 μM) of synthetic urushiol C15:0, C15:1, C15:2, or C15:3 for 5 days. Concentrations of IL-17A in supernatants were measured by ELISA (n=3, 3 independent experiments). (**c**, **d**) Mice were immunized with urushiol C15:2. (**c**) Ear swelling in wild-type and CD1aTg mice on day 2 after challenge (4-7 mice per group, 4 independent experiments). (**d**) Skin LCs were pulsed with C15:2 urushiol, and co-cultured with dLN $CD4^{+}$ T cells for 3 days in the presence or absence of anti-CD1a antibody. Concentrations of IL-17A in supernatants were measured by ELISA (n=3, 2 independent experiments, N.D., not detectable). Error bars represent s.e.m. * P<0.05, ** P<0.01; N.S., not significant, using Student's t-test.

Figure 6 CD1a binds and displays urushiol (C15:2) in its antigen-binding cleft. (**a**) Molecular interactions of urushiol (C15:2) with CD1a. Superposition of the CD1a-urushiol binary complex (in grey) and the complex of TCR-CD1a-endogenous lipid (in light blue) (PDB code: 4X6D). (**b**) Extracted ion chromatograms (Q1-Q3 transition) of urushiol C15:2 synthetic standard (in black), purified recombinant CD1a loaded with urushiol (in green), and crystal of CD1a-urushiol C15:2 (in red). (**c**) Accurate mass spectra for urushiol extracts comparing predicted molecular weight and isotope distribution pattern. (*i*) urushiol C15:2 theoretical mass, (*ii*) urushiol C15:2 synthetic standard, (*iii*) purified CD1a-urushiol C15:2 soluble extract, and (*iv*) CD1a-urushiol C15:2 binary complex crystal.

Figure 7 CD1a is a novel target for treatment of psoriatic inflammation. (**a**, **b**) Imiquimod (IMQ) was applied on ears of wild-type and CD1aTg mice for 6 days. (**a**) Representative hematoxylin and eosin stainings of tissue sections, and photographs of ears on day 7. Black arrows indicate epidermal thickening. Scale bar: 100 μm. (**b**) Ear swelling on day 7 (n=5, 5 independent experiments), *** P <0.001, using Student's t-test. (**c**-**e**) IMQ was applied on ears of wild-type, CD1aTg, and CD1aTg mice injected with either isotype or anti-CD1a antibody for 6 days. (**c**) Ear swelling (n=6-8 per group), (**d**) frequencies of Gr-1^{high}CD11b^{high} granulocytes and TCR-β^{+}CD4^{+} cells among live CD45^{+} cells, and (**e**) absolute cell numbers of IL-17A-, IL-17F-, and IL-22-producing CD4^{+} T cells isolated from challenged ears (n=3 per group, 3 independent experiments). (**f**) dLN CD4^{+} T cells of wild-type and CD1aTg mice treated or non-treated with IMQ for 6 days were stimulated by plate-bound CD1a loaded with fatty acid (FA), squalene (SQ), wax ester (WE), or triacylglycerol (TAG) for 5 days. Concentrations of IL-17A in supernatants were measured by ELISA (n=3, 3 independent experiments). (**g**) Memory T cells were isolated from patients with active psoriasis (n=6), or healthy donors (n=6), and cocultured with autologous monocyte-derived DCs in the presence or absence of anti-CD1a or isotype for 3 days. Concentrations of IL-17A and IL-22 in supernatants were determined by ELISA. Error bars represent s.e.m. * P <0.05, ** P <0.01, *** p<0.001, **** p<0.0001, using one-way ANOVA and multiple comparisons.

Supplementary Figure 1 Cytokine pattern in skin in response to urushiol. Mice were sensitized and challenged with urushiol. Quantitative real-time PCR was performed to analyze cytokine gene expression in the ear tissue obtained 2 days after challenge. Results are presented as fold increases over vehicle-treated ears from wild-type mice. Error bars represent s.e.m., n=3. Results are representative of 2 independent experiments.

Supplementary Figure 2 CD1a suppresses contact hypersensitivity mediated by IFN-γ-producing cells. Mice were sensitized with 0.5% DNFB by painting on the abdomen on day 0, and challenged with either 0.2% DNFB or vehicle on ears 5 days after sensitization. (**a**) Ear swelling after challenge. (**b**) Frequencies of Gr-1^{high}CD11b^{high} granulocytes (left), CD4$^+$ and CD8$^+$ T cells among live CD45$^+$TCRβ$^+$ cells (middle), and IL-17A$^+$ or IFN-γ$^+$ cells among TCRβ$^+$ cells (right). (**c**) Absolute cell numbers of CD8 or CD4 αβT cells, IFN-γ- or IL-17A-producing cells in ears. Error bars represent s.e.m. Results are representative of 3 independent experiments (n=3 per group for each experiment). ** P<0.01, *** P<0.001, using Student's t-test.

Supplementary Figure 3 Vβ TCR subfamily profile in skin and thymus. (**a-e**) Ear cells or thymocytes were isolated from wild-type or CD1aTg mice 2 days after urushiol C15:2 or vehicle challenge and analyzed for 15 different Vβ TCR subfamilies. Relative contribution of each Vβ$^+$ cell subset among CD45$^+$CD3$^+$CD4$^+$ T cells is presented in bar graphs. (**a**) Vβ TCR repertoire in urushiol-treated skin. (**b**) Frequencies of IL-17A$^+$ cells among Vβ2$^+$ or Vβ4$^+$ CD4$^+$ T cells in ear. Error bars represent s.e.m. (**c**) Frequencies of Vβ2$^+$ or Vβ4$^+$ cells in ears from CD1aTg versus CD1aTg mice injected with anti-CD1a antibody. (**d**) Vβ TCR repertoire in vehicle-treated skin. Error bars represent s.e.m. (**e**) Vβ TCR repertoire in thymus. Results are representative of 2-3 independent experiments. * P<0.05, ** P<0.01; N.S., not significant, using Mann-Whitney test.

Supplementary Figure 4 Crystal structure of the CD1a-urushiol complex. (**a**) Overall cartoon representation of the binary crystal structure of CD1a-urushiol C15:2. (**b**) Top view of the molecular surface of the α1- and α2- domains of CD1a (in grey) and the bound urushiol shown

as spheres (in magenta). (**c**) Fo-Fc electron density map (yellow orange) of urushiol contoured at 2.2 σ level. (**d**) 2Fo-Fc electron density map (in blue) of urushiol contoured at 0.8 σ level.

Figure 1

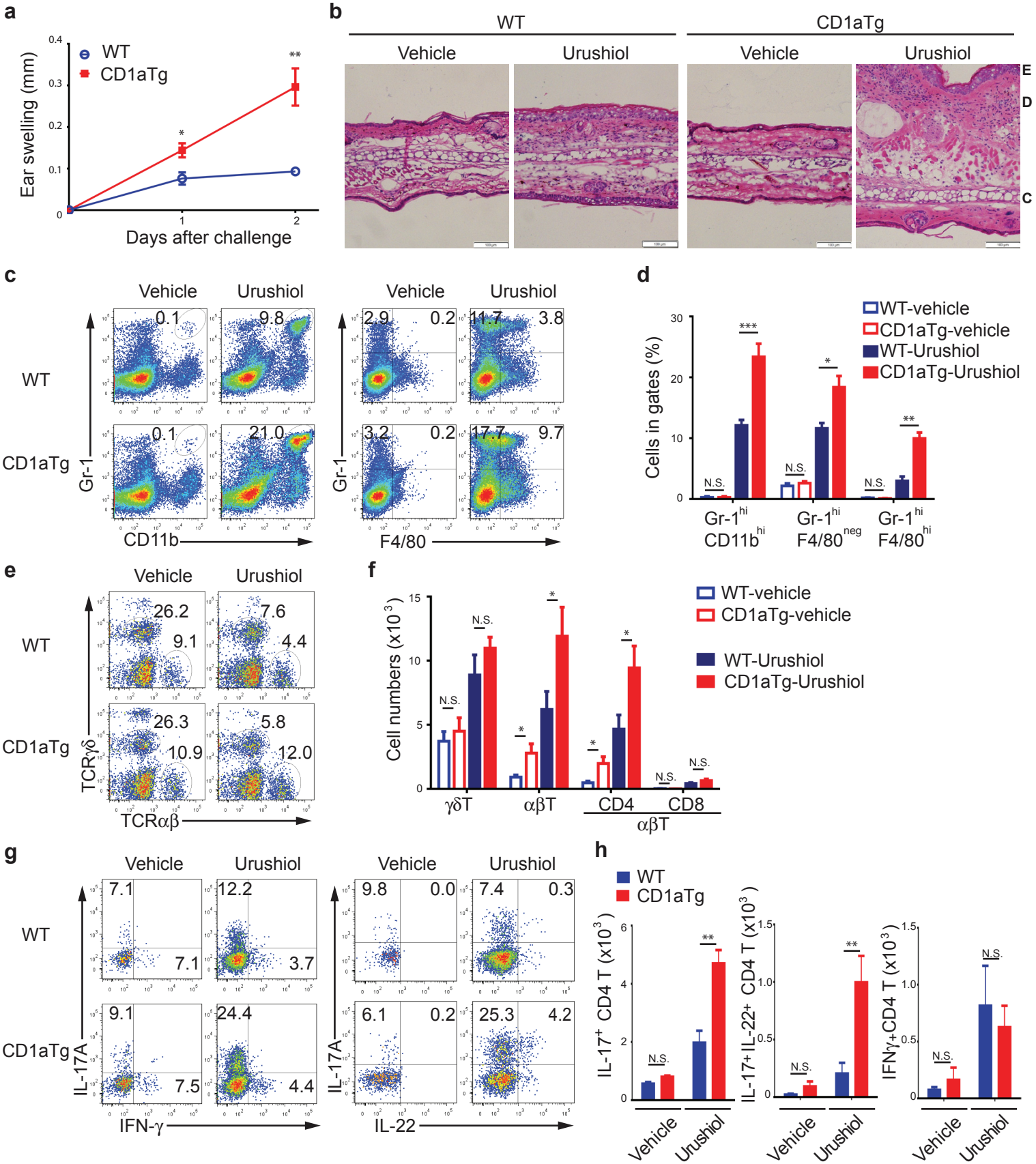
a
Ear swelling (mm)
WT
CD1aTg
Days after challenge
b
WT
CD1aTg
Vehicle
Urushiol
E
D
C
c
Vehicle
Urushiol
WT
CD1aTg
Gr-1
CD11b
F4/80
d
Cells in gates (%)
WT-vehicle
CD1aTg-vehicle
WT-Urushiol
CD1aTg-Urushiol
N.S.
Gr-1hi CD11bhi
Gr-1hi F4/80neg
Gr-1hi F4/80hi
e
TCRγδ
TCRαβ
f
Cell numbers (x10 3)
γδT
αβT
CD4
CD8
g
IL-17A
IFN-γ
IL-22
h
IL-17+ CD4 T (x10 3)
IL-17+IL-22+ CD4 T (x10 3)
IFNγ+CD4 T (x10 3)

Figure 2

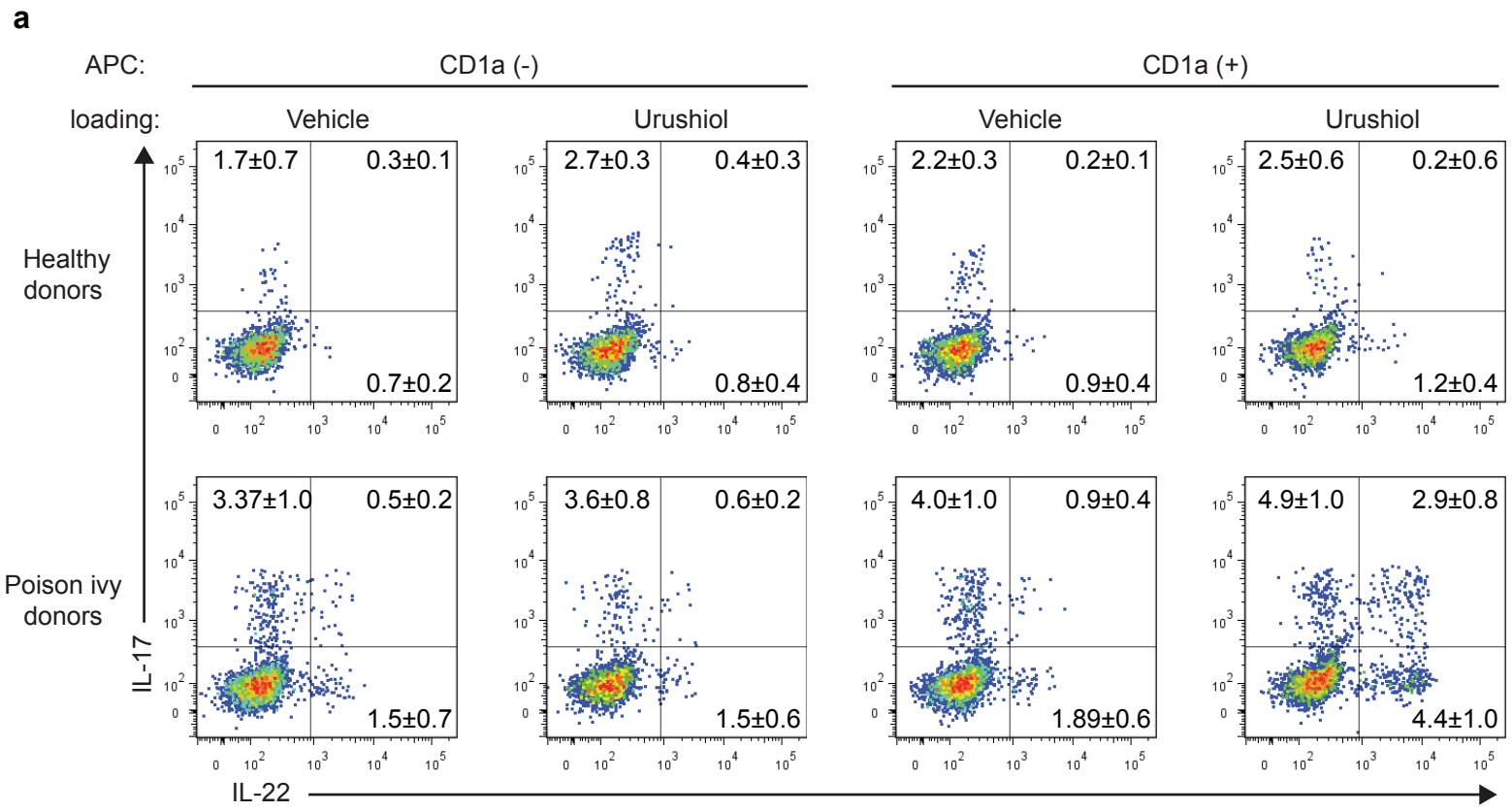
a
APC:
CD1a (-)
CD1a (+)
loading:
Vehicle
Urushiol
Vehicle
Urushiol
Healthy donors
Poison ivy donors
1.7±0.7
0.3±0.1
0.7±0.2
2.7±0.3
0.4±0.3
0.8±0.4
2.2±0.3
0.2±0.1
0.9±0.4
2.5±0.6
0.2±0.6
1.2±0.4
3.37±1.0
0.5±0.2
1.5±0.7
3.6±0.8
0.6±0.2
1.5±0.6
4.0±1.0
0.9±0.4
1.89±0.6
4.9±1.0
2.9±0.8
4.4±1.0
IL-17
IL-22

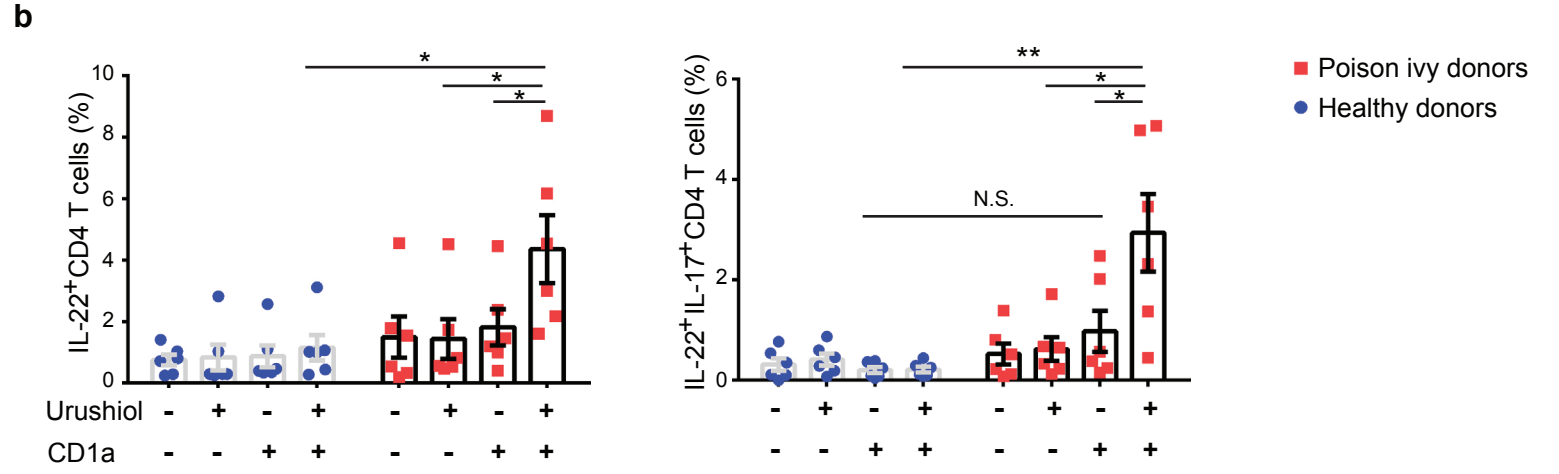
b
IL-22+CD4 T cells (%)
IL-22+IL-17+CD4 T cells (%)
N.S.
Urushiol
CD1a
Poison ivy donors
Healthy donors

Figure 3

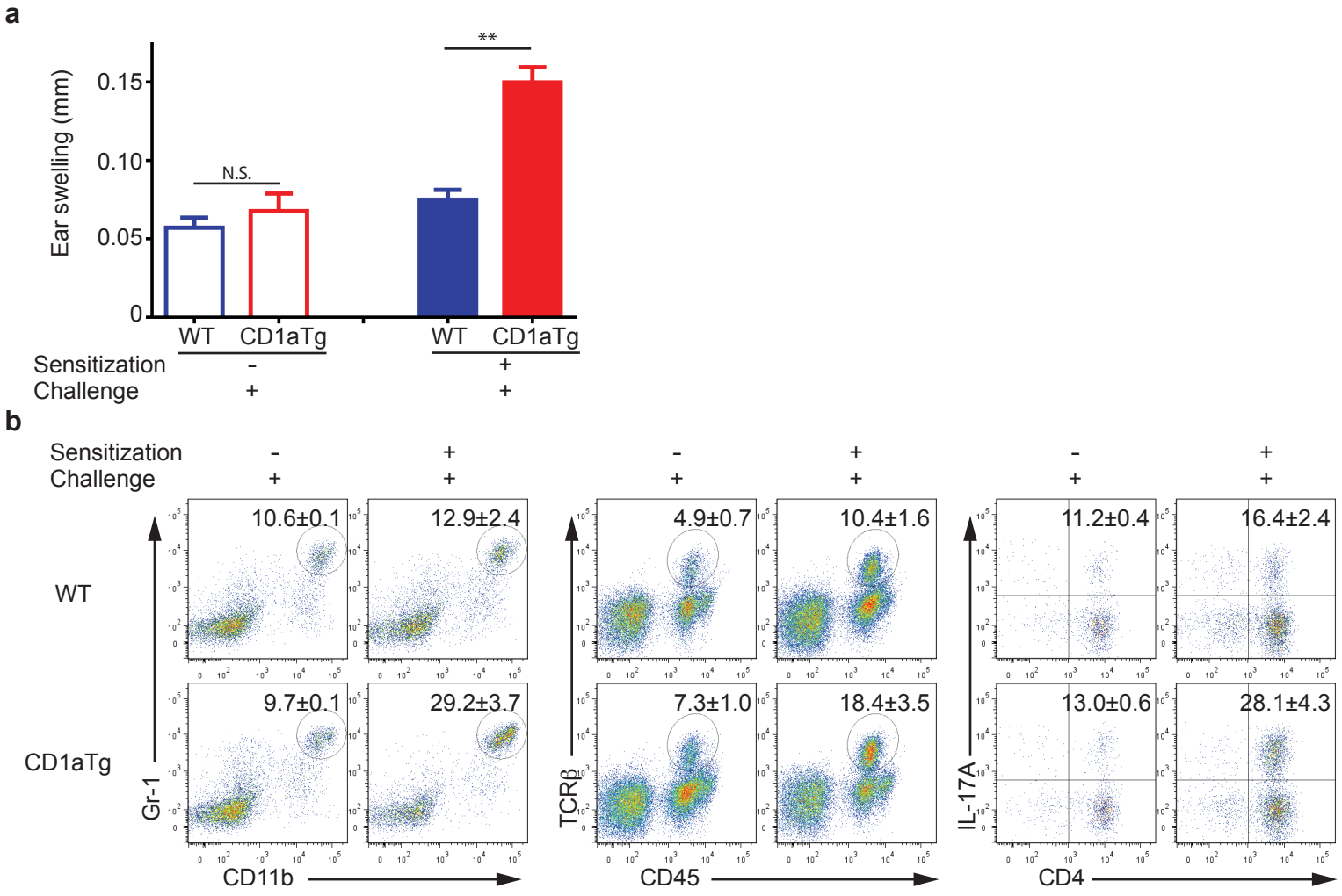
a
Ear swelling (mm)
0.15
0.10
0.05
0
**
N.S.
WT
CD1aTg
WT
CD1aTg
Sensitization
-
+
Challenge
+
+
b
Sensitization
-
+
-
+
-
+
Challenge
+
+
+
+
+
+
WT
CD1aTg
10.6±0.1
12.9±2.4
9.7±0.1
29.2±3.7
4.9±0.7
10.4±1.6
7.3±1.0
18.4±3.5
11.2±0.4
16.4±2.4
13.0±0.6
28.1±4.3
Gr-1
CD11b
TCRβ
CD45
IL-17A
CD4

Figure 4

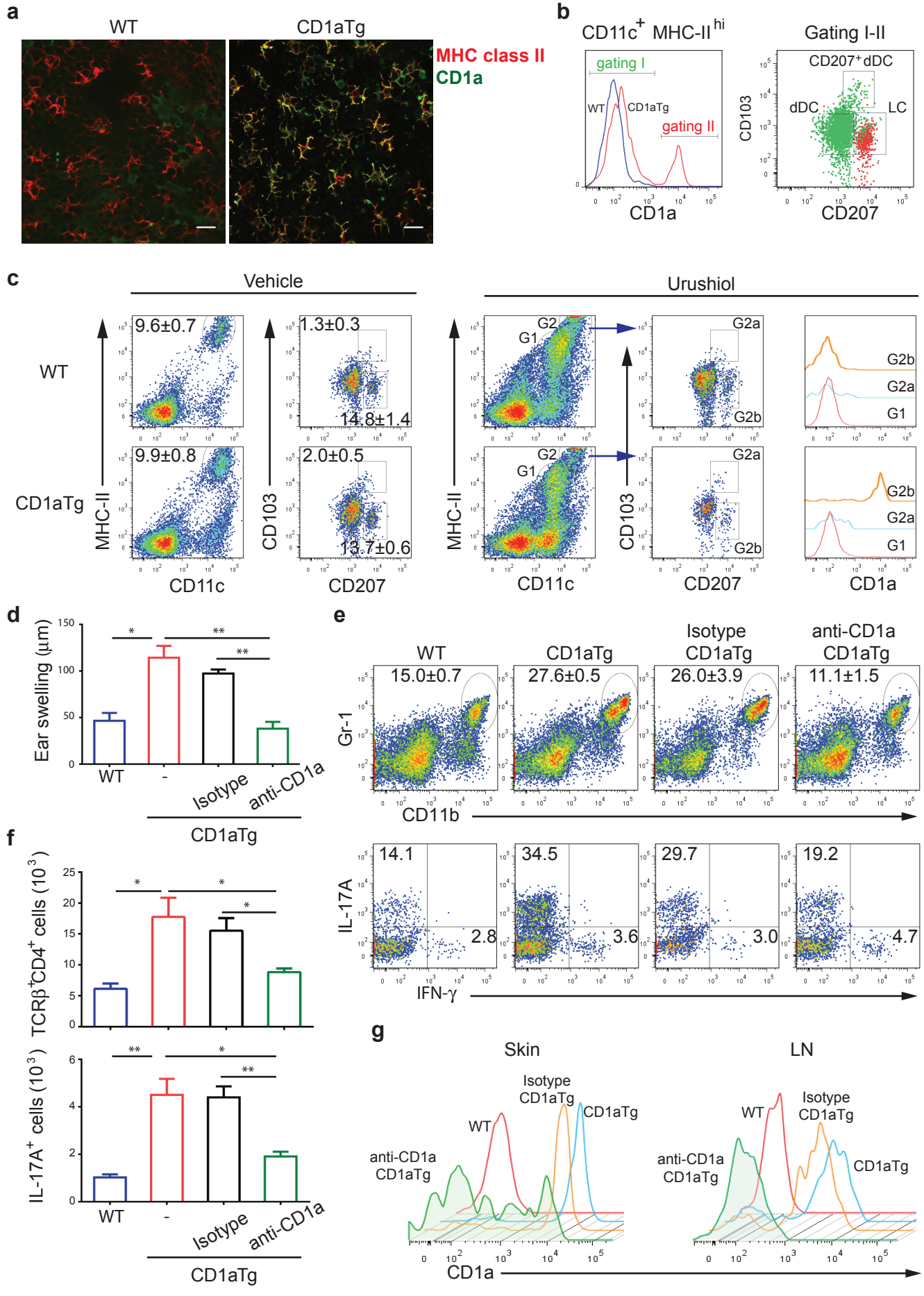
a
WT
CD1aTg
MHC class II
CD1a
b
CD11c+ MHC-II hi
gating I
gating II
WT
CD1aTg
CD1a
Gating I-II
CD207+dDC
dDC
LC
CD103
CD207
c
Vehicle
Urushiol
WT
CD1aTg
9.6±0.7
1.3±0.3
14.8±1.4
9.9±0.8
2.0±0.5
13.7±0.6
MHC-II
CD11c
CD103
CD207
G2
G1
G2a
G2b
CD1a
d
Ear swelling (μm)
WT
-
Isotype
anti-CD1a
CD1aTg
e
WT
CD1aTg
Isotype CD1aTg
anti-CD1a CD1aTg
15.0±0.7
27.6±0.5
26.0±3.9
11.1±1.5
Gr-1
CD11b
14.1
34.5
29.7
19.2
2.8
3.6
3.0
4.7
IL-17A
IFN-γ
f
TCRβ+CD4+ cells (10^3)
IL-17A+ cells (10^3)
WT
-
Isotype
anti-CD1a
CD1aTg
g
Skin
LN
Isotype CD1aTg
WT
CD1aTg
anti-CD1a CD1aTg
CD1a

Figure 5

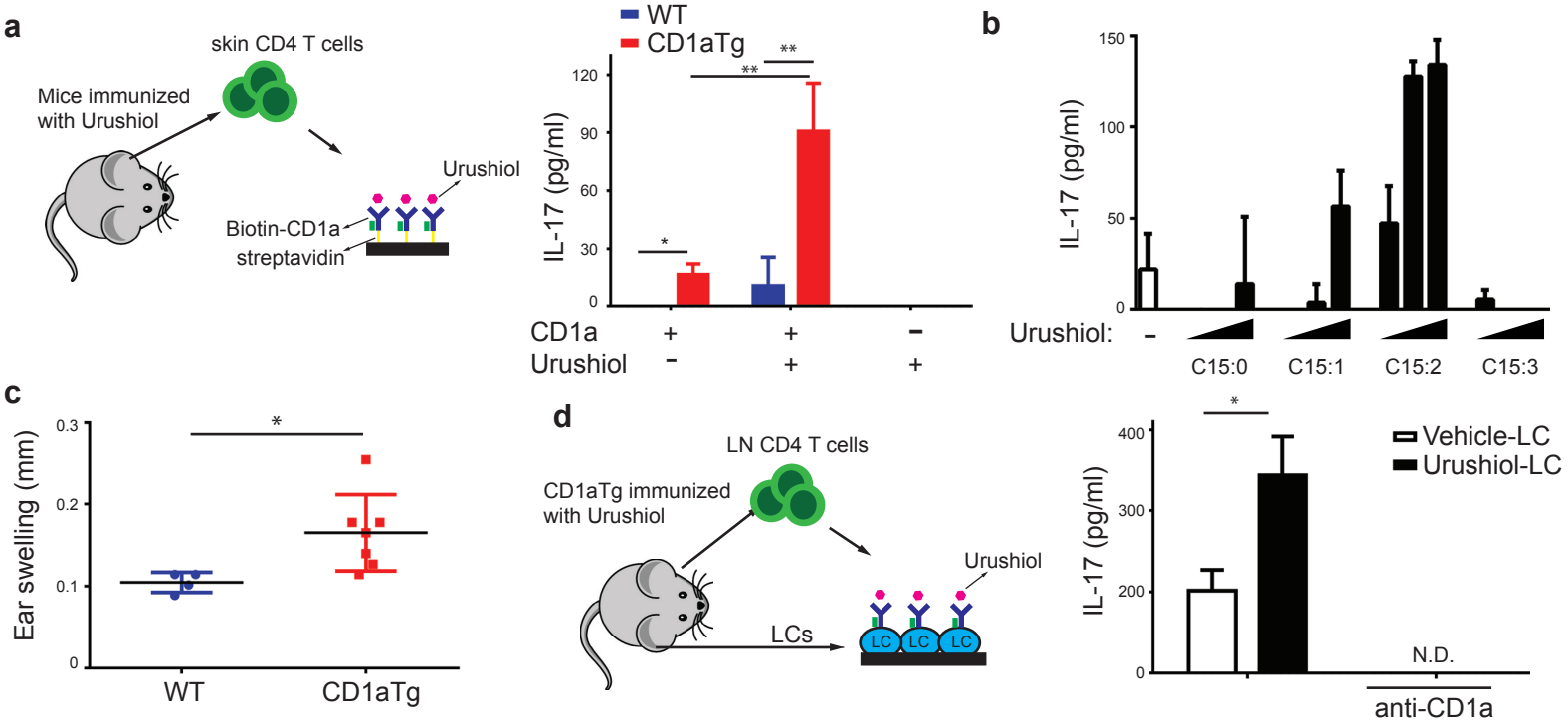
a
skin CD4 T cells
Mice immunized
with Urushiol
Urushiol
Biotin-CD1a
streptavidin
WT
CD1aTg
IL-17 (pg/ml)
CD1a
Urushiol
b
IL-17 (pg/ml)
Urushiol:
C15:0
C15:1
C15:2
C15:3
c
Ear swelling (mm)
WT
CD1aTg
d
LN CD4 T cells
CD1aTg immunized
with Urushiol
Urushiol
LCs
LC
Vehicle-LC
Urushiol-LC
N.D.
anti-CD1a

Figure 6

a

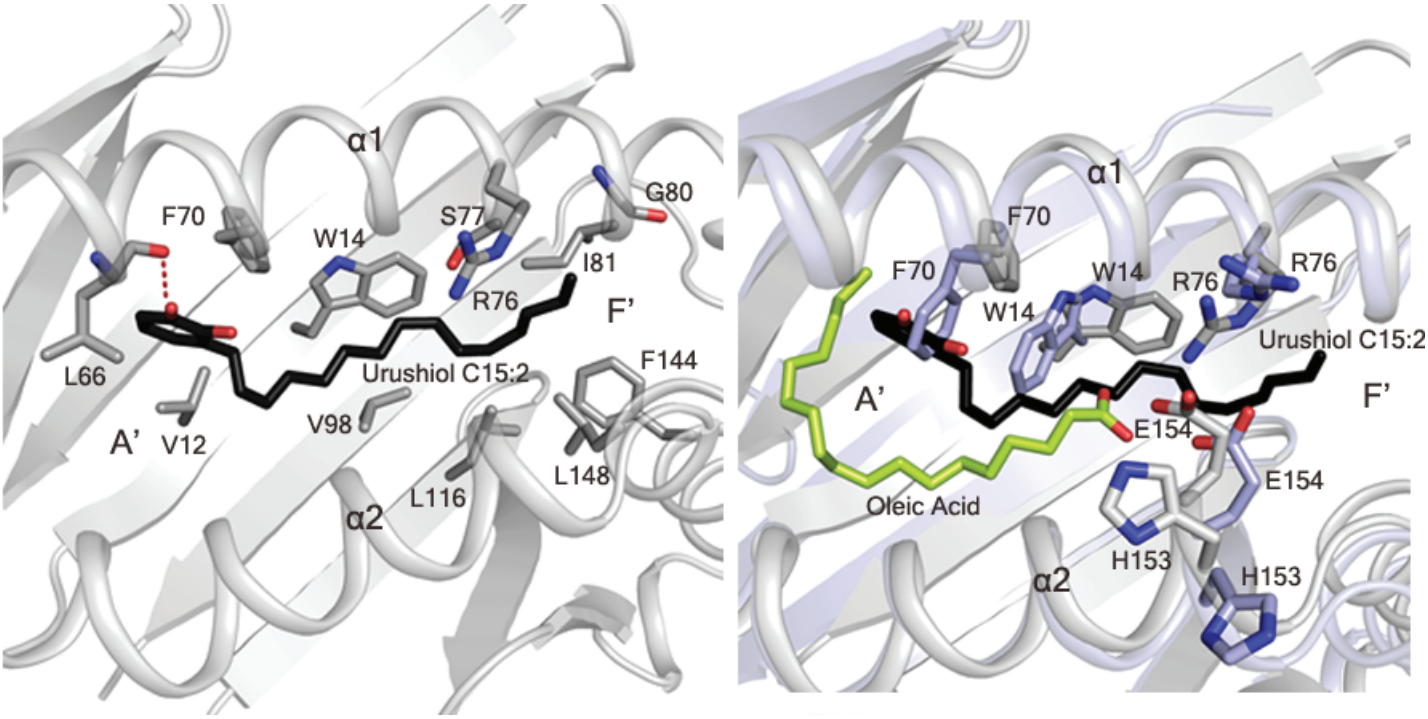
α1
F70
W14
S77
G80
I81
R76
F'
L66
Urushiol C15:2
F144
A'
V12
V98
L148
L116
α2
α1
F70
F70
W14
W14
R76
R76
Urushiol C15:2
A'
F'
E154
E154
Oleic Acid
H153
H153
α2

b

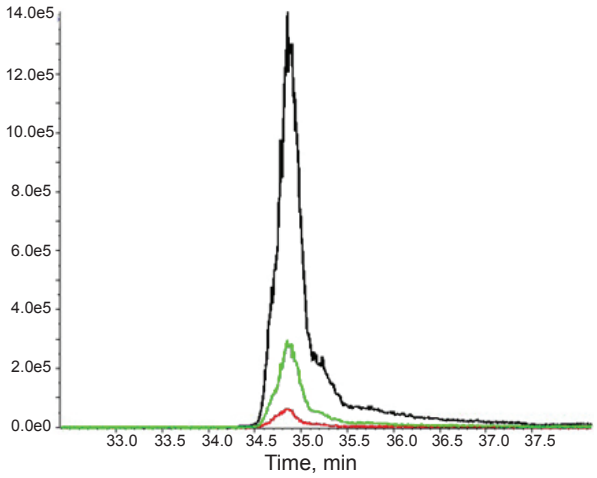
14.0e5
12.0e5
10.0e5
8.0e5
6.0e5
4.0e5
2.0e5
0.0e0
33.0 33.5 34.0 34.5 35.0 35.5 36.0 36.5 37.0 37.5
Time, min

c

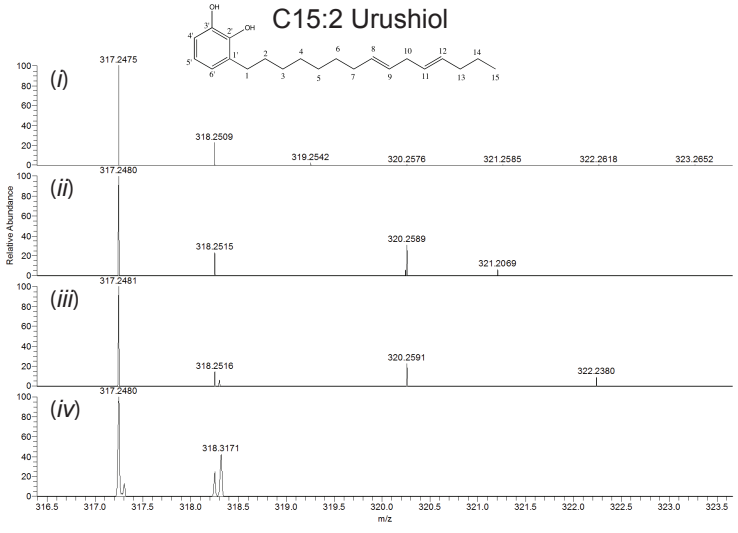
C15:2 Urushiol
(i)
317.2475
318.2509
319.2542
320.2576
321.2585
322.2618
323.2652
(ii)
317.2480
318.2515
320.2589
321.2069
(iii)
317.2481
318.2516
320.2591
322.2380
(iv)
317.2480
318.3171
Relative Abundance
m/z

Figure 7

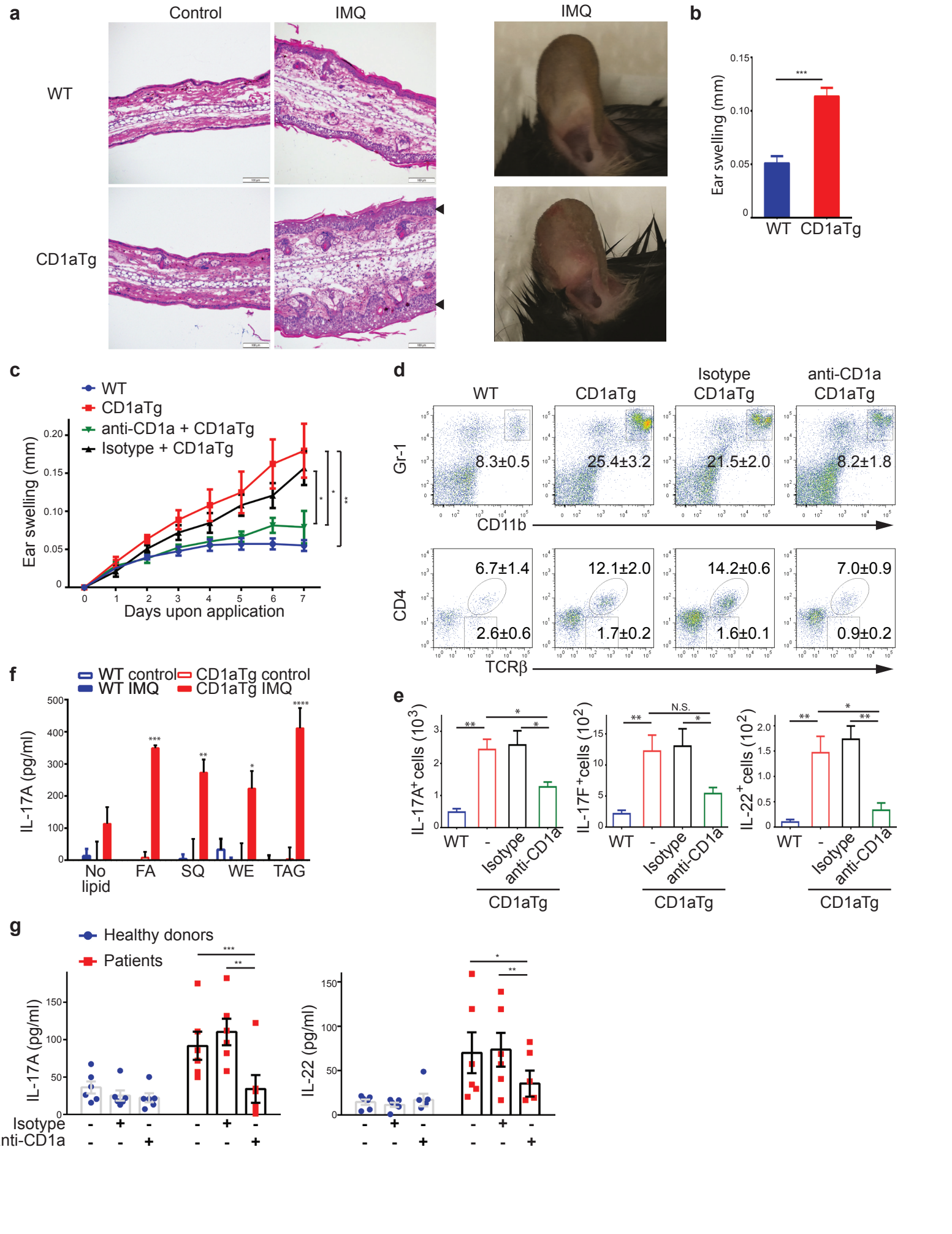
a
Control
IMQ
IMQ
WT
CD1aTg
b
Ear swelling (mm)
0.15
0.10
0.05
0
***
WT
CD1aTg
c
WT
CD1aTg
anti-CD1a + CD1aTg
Isotype + CD1aTg
Ear swelling (mm)
0.20
0.15
0.10
0.05
0
0 1 2 3 4 5 6 7
Days upon application
* * **
d
WT
CD1aTg
Isotype CD1aTg
anti-CD1a CD1aTg
Gr-1
8.3±0.5
25.4±3.2
21.5±2.0
8.2±1.8
CD11b
CD4
6.7±1.4
12.1±2.0
14.2±0.6
7.0±0.9
2.6±0.6
1.7±0.2
1.6±0.1
0.9±0.2
TCRβ
e
IL-17A+ cells (10^3)
IL-17F+cells (10^2)
IL-22+cells (10^2)
N.S.
WT
-
Isotype
anti-CD1a
CD1aTg
f
WT control
CD1aTg control
WT IMQ
CD1aTg IMQ
IL-17A (pg/ml)
500
400
300
200
100
0
***
**
*
****
No lipid
FA
SQ
WE
TAG
g
Healthy donors
Patients
IL-17A (pg/ml)
IL-22 (pg/ml)
Isotype
anti-CD1a

Supplementary Figure 1

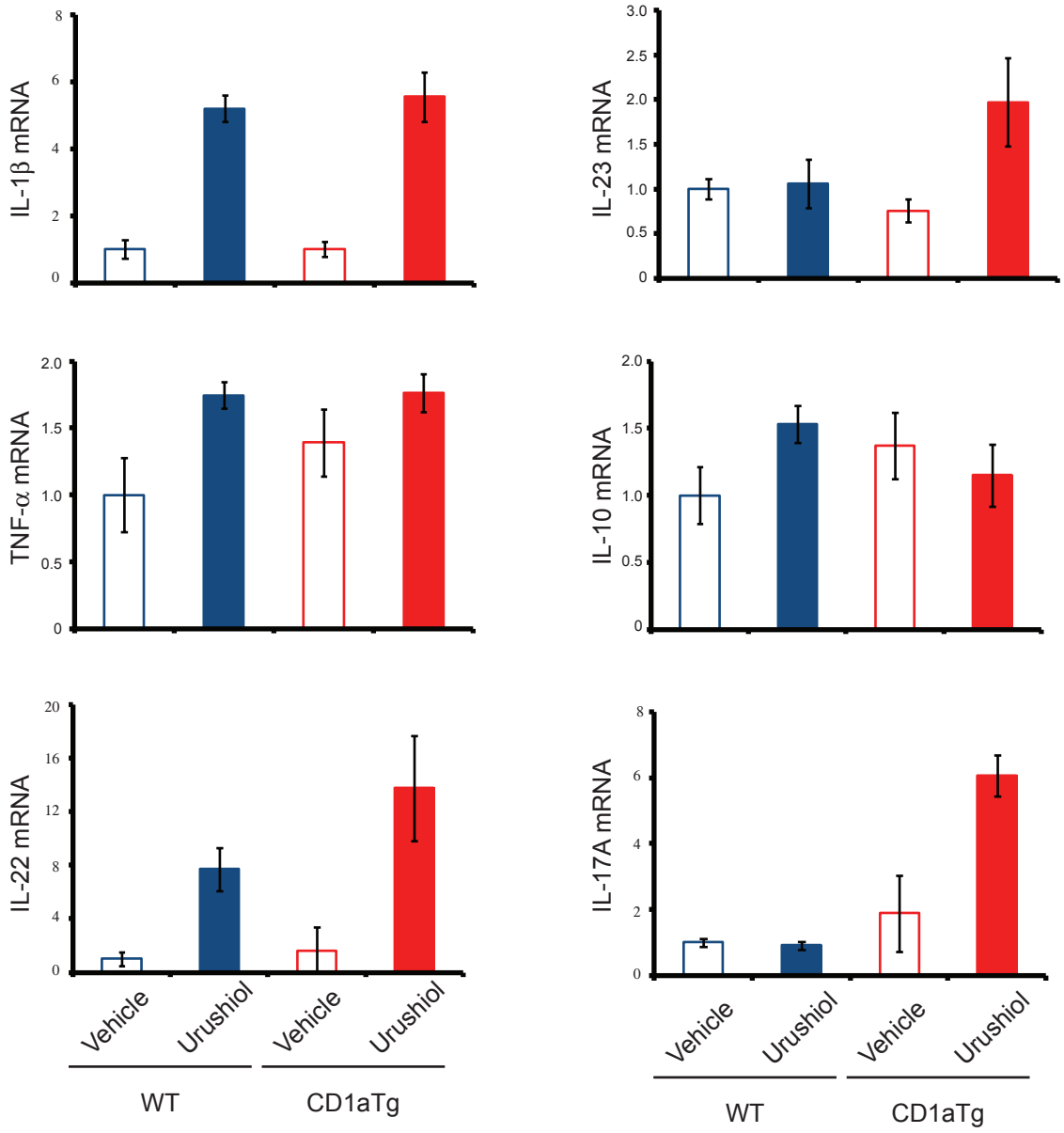

Supplementary Figure 2

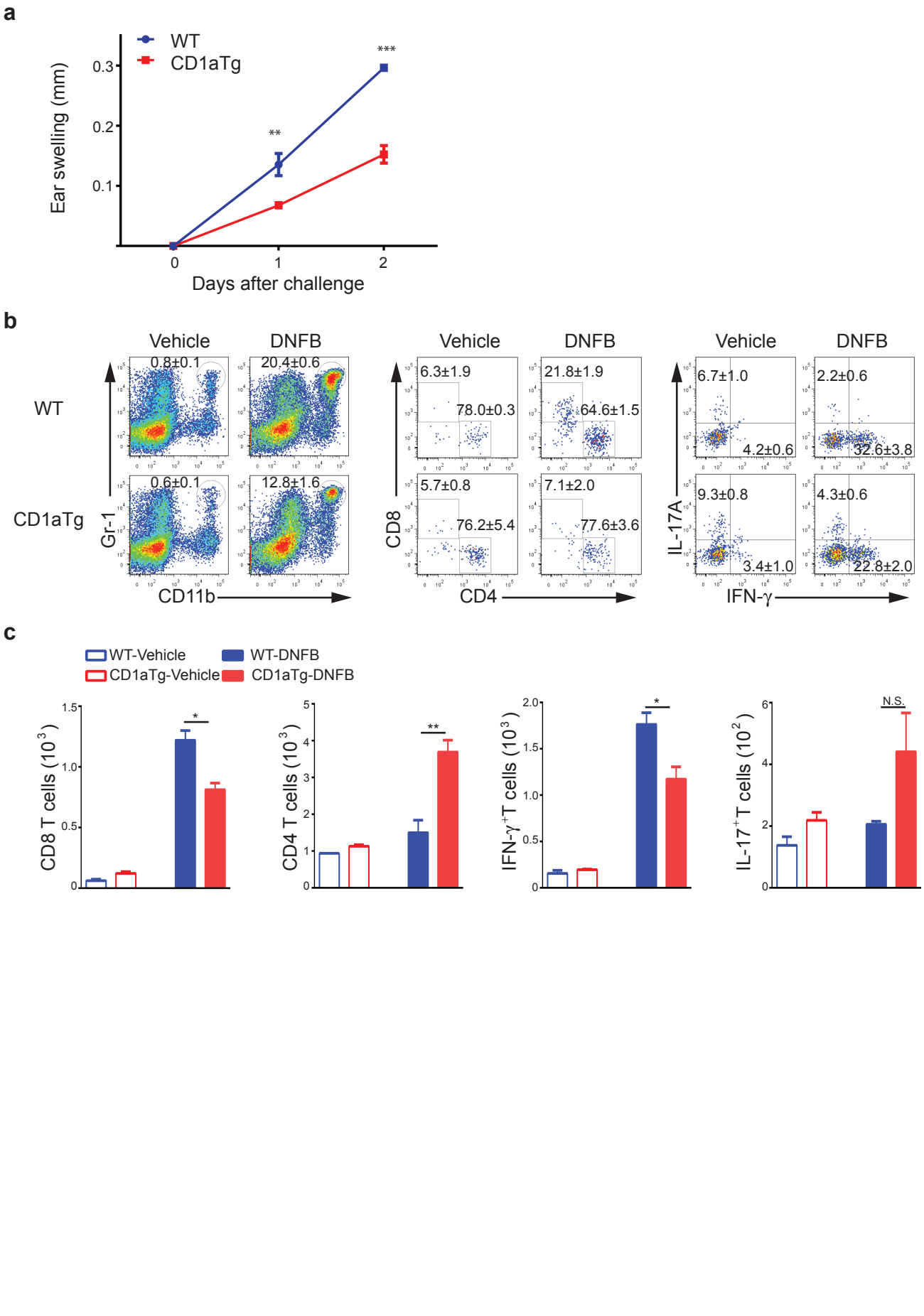

Supplementary Figure 3

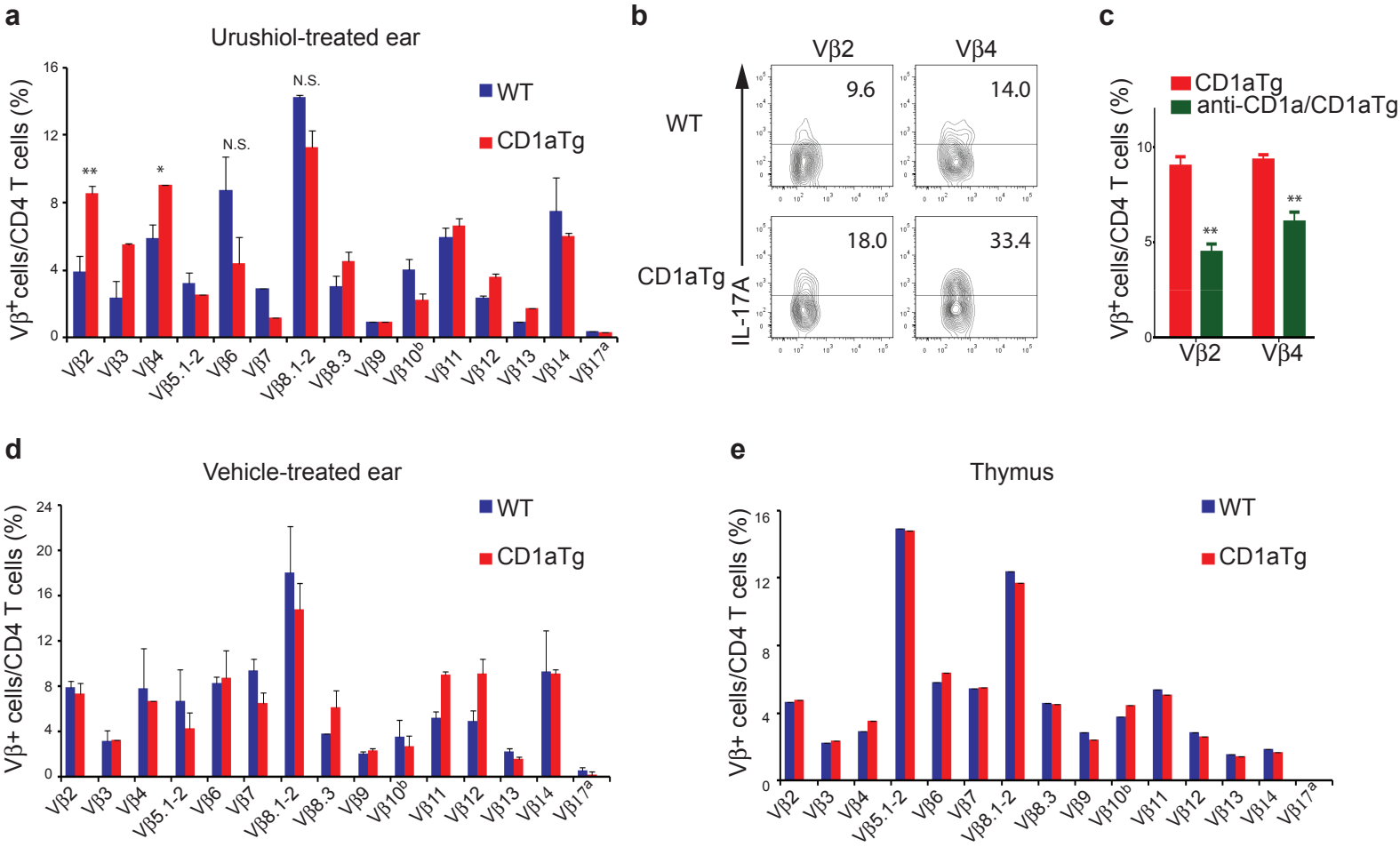

Supplementary Figure 4

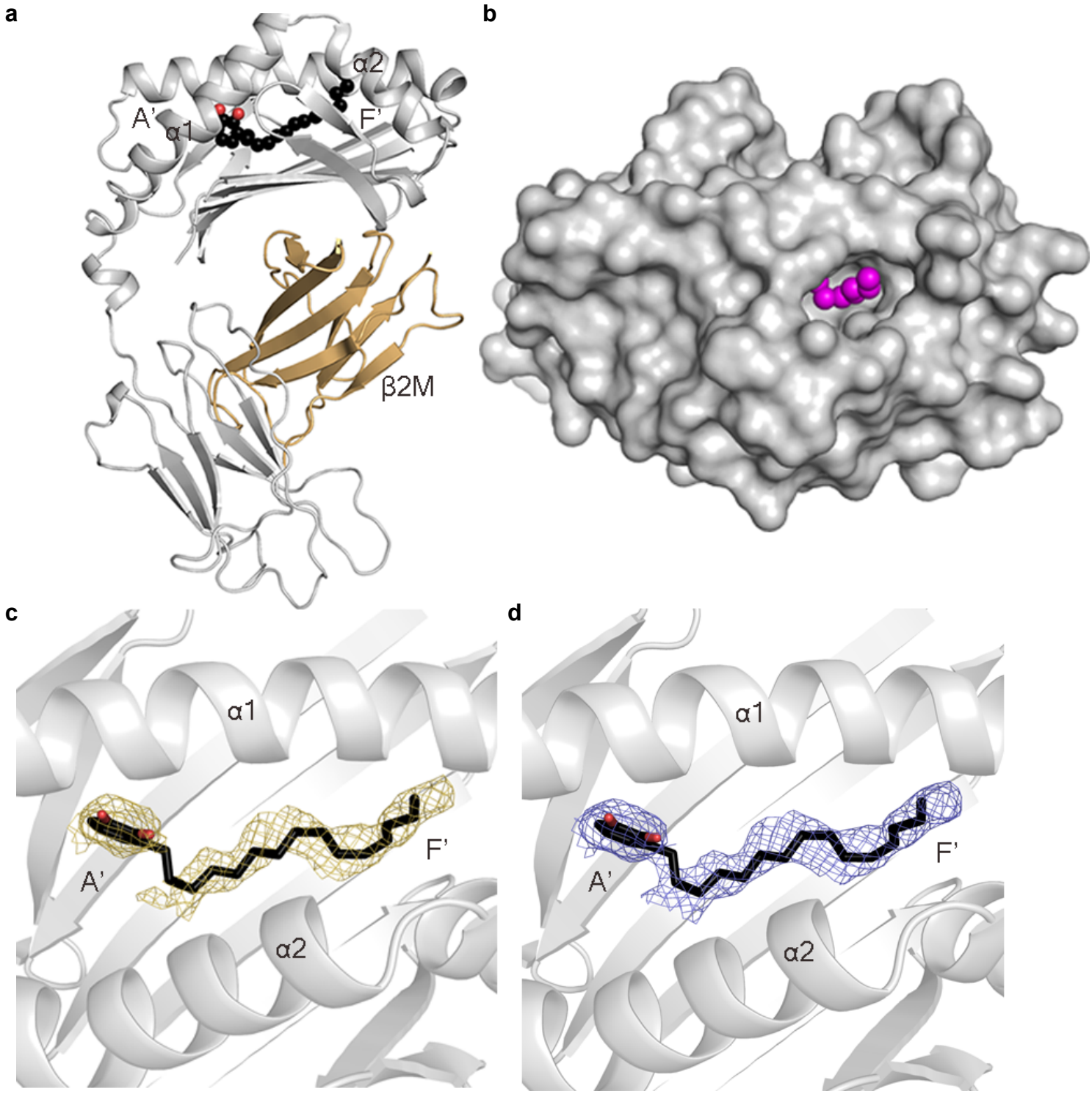

Supplementary Table 1 Data collection and refinement statistics

	CD1a-Urushiol
Data collection	
Temperature	100K
Resolution limits (Å)	45.8-1.86 (1.9-1.86)
Space Group	$P2_12_12_1$
Cell dimensions (Å)	*a*=42.2, *b*=90.3, *c*=106.2 α=β=γ=90.00°
Total N°. observations	506717 (31388)
N°. unique observations	35008 (2139)
Multiplicity	14.5 (14.7)
Data completeness	100 (100)
Wilson B-factors (Å^2)	22.9
I/σ_1	15.5 (3.7)
$R_{p.i.m}$ [1] (%)	3.8 (36)
Refinement statistics	
R_{factor} [2] (%)	18.6
R_{free} [3] (%)	21.6
Non hydrogen atoms	
- Protein	2927
- Water	250
- Heterogen	23
Ramachandran plot (%)	
- Most favoured	97.55
- Allowed	2.17
B-factors (Å^2)	
- Average main chain	29.3
- Average side chain	35.4
- Urushiol	55.3
rmsd bonds (Å)	0.010
rmsd angles (°)	1.00

[1] $R_{p.i.m} = \Sigma_{hkl} [1/(N-1)]^{1/2} \Sigma_i | I_{hkl,\,i} - \langle I_{hkl} \rangle | / \Sigma_{hkl} \langle I_{hkl} \rangle$

[2] $R_{factor} = (\Sigma | |F_o| - |F_c| |) / (\Sigma |F_o|)$ - for all data except as indicated in footnote 3.

[3] 5% of data was used for the R_{free} calculation

Values in parentheses refer to the highest resolution bin.

Supplementary Table 2 CD1a contacts with Urushiol

CD1a residues	Urushiol atoms	Bond type
Val12	C1, C2, C3, C6’	VDW
Trp14	C8, C9	VDW
Leu66	C3’, O3’	VDW
Leu66-O	O3’	HB
Phe70	C1, C1’, C2’, C3’, O2’, O3’	VDW
Arg76	C15	VDW
Ser 77	C8, C9, C10, C13, C14, C15	VDW
Gly80	C15	VDW
Ile81	C12	VDW
Val98	C5	VDW
Leu116	C11	VDW
Phe144	C12	VDW
Leu148	C12, C13, C14	VDW

HB: Hydrogen bond, VDW: Van der Waals, SB: salt bridge. Cut-off at 4 Å for VDW interactions and 3.5 Å for HB.